Nanoscale

Topological quantum devices: a review

Journal:	*Nanoscale*
Manuscript ID	NR-REV-03-2023-001288.R1
Article Type:	Review Article
Date Submitted by the Author:	21-Jun-2023
Complete List of Authors:	Jin, Kyung-Hwan; IBS, Center for Artificial Low Dimensional Electronic Systems Jiang, Wei; Beijing Institute of Technology Sethi, Gurjyot; The University of Utah, Department of Materials Science and Engineering Liu, Feng; University of Utah, Department of Materials Science

Topological quantum devices: a review

Kyung-Hwan Jin[1,†], Wei Jiang[2,†], Gurjyot Sethi[3,†] and Feng Liu[3,*]

[1]Center for Artificial Low Dimensional Electronic Systems, Institute for Basic Science (IBS), Pohang 37673, Republic of Korea

[2]School of Physics, Beijing Institute of Technology, Beijing 100081, China

[3]Department of Materials Science and Engineering, University of Utah, Salt Lake City, Utah 84112, United States

†These authors contributed equally to the work

*e-mail: fliu@ eng.utah.edu

Abstract

The introduction of the concept of topology into condensed matter physics has greatly deepened our fundamental understanding of transport properties of electrons as well as all other forms of quasi particles in solid materials. It has also fostered a paradigm shift from conventional electronic/optoelectronic devices to novel quantum devices based on topology-enabled quantum device functionalities that transfer energy and information with unprecedented precision, robustness, and efficiency. In this article, the recent research progress in topological quantum devices is reviewed. We first outline the topological spintronic devices underlined by the spin-momentum locking property of topology. We then highlight the topological electronic devices based on quantized electron and dissipationless spin conductivity protected by topology. Finally, we discuss quantum optoelectronic devices with topology-redefined photoexcitation and emission. The field of topological quantum devices is only at its infancy, we envision many significant advances in the near future.

1. Introduction

The concept of topology was first introduced into condensed matter physics in the early 80s of the last century to explain the quantum Hall effect (QHE)[1]. It was shown that quantized electron conductivity can result from non-trivial electron band topology. This has not only revolutionized our fundamental understanding of electron transport behavior, but also afforded new device concepts with the highest possible precision, i.e., measurement of fine-structure of atoms, because the quantized conductivity depends on only fundamental physical constants (e, h, π)[2]. However, a super high magnetic field and extremely low temperature required for the QHE have limited its further applications, until when the concept of topology was introduced in lattice models[3] and solid-state materials[4-6].

Over the past 18 years or so, the understanding of topological concept in condensed matters is significantly advanced along with the continued discovery of various topological materials[7-11] (see Fig. 1). As a new type of "quantum conductor", 2D/3D topological insulator (TI) is a bulk insulator but an edge/surface conductor, where the edge/surface conductance is quantized, in accordance with a bulk-boundary correspondence protected by a nontrivial Z_2 topology of bulk electronic wave functions[7]. A TI can be viewed as two copies of Chern insulator[12], one for each spin channel. Their nontrivial topology is characterized with a non-zero Z_2 (±1) invariant or integer Chern number for one spin channel, which can be calculated by integration of Berry curvature of wave functions[7] over the Brillouin zone (BZ) for all the occupied bands below the topological gap. On the other hand, a topological Dirac/Weyl semimetal is a weak topological non-magnetic/magnetic bulk conductor with a vanishing density of states (DOS) at the Fermi level, where the Dirac and Weyl points represent a Berry flux center, i.e., a divergent point of Berry curvature for the valence (conduction) bands below (above) the Dirac/Weyl point having opposite chirality (opposite pseudospin), such as the upper (lower) Dirac cones of graphene. In general, a TI can arise from gap opening at the Dirac point or band inversion of a narrow-gap semiconductor featured with two band-edge states of opposite parity (such as *s*- and *p*-states), induced by spin-orbit coupling (SOC)[13-15]. Another prominent feature of 2D/3D TI is that their topological edge/surface states (TSSs) is helical, exhibiting a spin-momentum locking property due to SOC, which constrains the orientation of spins perpendicular to that of momenta[16, 17].

Also, the topological concept has also been extended to topological crystalline insulator[18, 19] and high-order TI[20, 21], for which the nontrivial topology and bulk-boundary correspondence arise from protection of crystalline spatial symmetry[8, 22]. Furthermore, the single-particle concept of topology has been incorporated into correlated materials[23-25] and superconductors[26-29]. It has been shown that topological phenomena can also emerge in collective excitations, such as phonons[30, 31], magnons[32], and plasmons[33]. On the other hand, topological flat band (FB) presents another topological manifestation, in analogy to Landau level which is topological without band inversion; while a singular band touching point between a FB and a dispersion band can be viewed as a Berry flux center, in analogy to a Dirac point[11, 34-37]. Remarkably, the FB is dispersionless whose single-particle energy $E(\boldsymbol{k})$ is independent of momentum $\boldsymbol{k}$, so that the kinetic energy is completely quenched in the FB. Consequently, this macroscopically degenerate quantum-mechanical state is inherently a

strongly correlated state, offering an ideal platform to investigate exotic many-body quantum phenomena in association with topology[11], such as fractional quantum Hall effect[38-40], ferromagnetism[41-44], Wigner crystallization[45, 46], superconductivity[47-49], excitonic insulator[50] and Bose-Einstein condensates (BEC)[51-53]. Very interestingly, a new class of quantum semiconductors have been recently proposed, which have both a flat valence and conduction bands around the Fermi level, the so-called yin-yang FB of opposite chirality[50, 54]. In contrast with conventional semiconductors having parabolic band edges, yin-yang FBs are inherently topologically nontrivial and invoking strong electron-electron interaction, so that transport of fermionic carriers of electrons and holes, as well as bosonic excitons are quantum by nature. Such quantum semiconductors are expected to revive the "classical" semiconductor physics, leading to a paradigm shift of electronic and optoelectronic devices into the realm of quantum information and computation technologies.

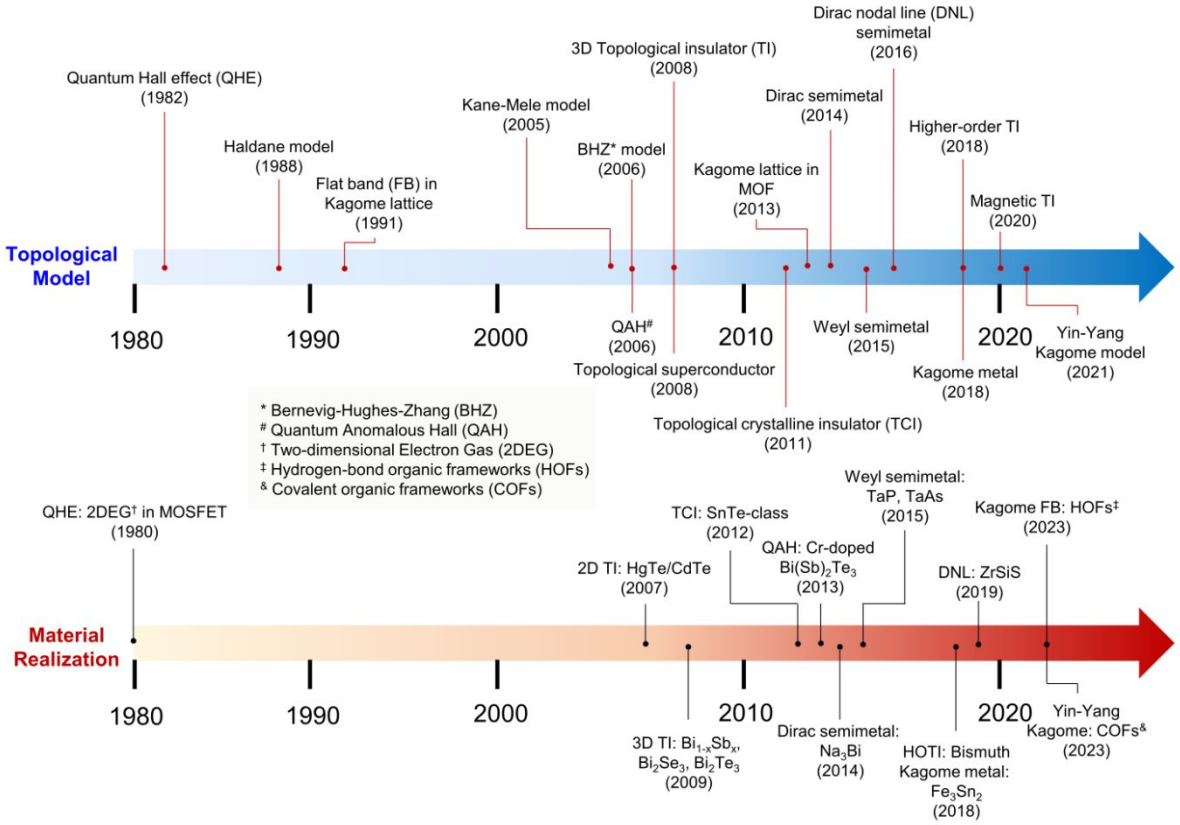

Fig. 1 Timeline of original discoveries of new concepts and materials in the field of topological materials.

Excitingly, the rise of topological materials opens a new door to topology-enabled quantum devices. It not only provides a new knob to manipulate the electronic states in conventional electronic, optoelectronic, and spintronic device settings, but has also fostered new quantum device concepts and platforms with unprecedented precision, robustness, and efficiency. For example, robust quantized conductivity renders transport signal with extremely high

precision[55]. The spin-momentum locking property prohibits elastic backscattering allowing creation of pure quantized spin current without heat dissipation[56, 57]. Topological superconductivity opens a new paradigm of fault-tolerant quantum computing[58]. As theoretical predictions of many topological phenomena have been characterized and confirmed experimentally, using transport measurement, scanning tunnelling microscopy/spectroscopy, angle-resolved photoemission spectroscopy and magneto-optical spectroscopy, significant efforts have also been made toward realizing topological quantum devices.

In this review, we recap the recent progress made in developing topological devices, by employing new topology-enabled physical phenomena as well as engineering approaches to manipulate these phenomena. We first discuss new physical concepts and applications in association with topological spintronic devices. Specifically, we will review works in charge-spin conversion, spin transport devices, and magnetic devices enabled by unique topological properties. We then discuss recent studies to extend application of topological materials to electronic devices, such as topological field-effect transistor and topological p-n junction. In addition, we briefly review the important role played by topology in optoelectronic device applications. In particular, we will introduce a new class of plasmonic topological materials, with promising applications in topological laser, and novel optoelectronic device employing topological FB systems.

2. Topological spintronic devices

In this section, we attempt to give an up-to-date overview of the research progress made in the fundamental physics and applications for topological spintronic devices. Spintronics has emerged as a promising field for advancing next-generation quantum devices with enhanced memory, processing capabilities, and reduced power consumption. These devices leverage the spin degree of freedom of electrons and/or holes, which can interact with their orbital moments. Traditionally, spin polarization in such devices is achieved through the use of magnetic layers as spin-polarizers or analyzers, or through the influence of SOC. However, by harnessing the unique topological properties of materials, it becomes feasible to create an intrinsic spin-polarized channel without magnetic fields or magnetic materials. In addition, the topologically protected spin channel allows for a long spin lifetime and spin diffusion length, which are useful in spin transistor and logic device applications. Recently, beyond the topological properties of electronic structure, new topological behaviors related to the topology of atomic structure, such as the dislocations and the nonsymmorphic crystal symmetry, are discovered. New forms of the SOC effect in specific atomic structure provide more effective means to manipulate spin transport properties.

We note that in the field of topological spintronic devices, several main challenges remain to be addressed. First, material selection is crucial, requiring the identification of materials with desired properties such as large topological energy gap, long spin coherence time, and efficient spin manipulation. Secondly, precise control and manipulation of spins in topological devices are essential. This involves utilizing the unique electronic structure of

topological materials and employing external perturbations such as electric field, magnetic field, mechanical strain, and optical control. Thirdly, reliable fabrication techniques are needed to create device structures and interfaces while preserving the spin-related properties of the materials. Scalable and low-cost production methods for large-scale topological materials are being explored. Finally, scaling up the fabrication of topological spintronic devices and integrating them into practical systems present significant challenges in terms of scalability, compatibility with existing technologies, and device integration. To address these challenges, extensive research has been conducted on various concepts and proposals for topological devices, and further studies on topological spintronic devices are ongoing.

This section is structured as follows. We begin with introducing the basic concept for generating pure spin current using 2D TI and the nanomechanical architecture for spin rectifying devices application. Then we discuss the efficient control and manipulation of spin degrees of freedom in magnetic TI structures. Next, we briefly review the unique spin structure in topological dislocations. Finally, we discuss the unidirectional spin textures and spin coherent properties in nonsymmorphic materials for novel multi-functional spin transistors.

2.1 Perfect spin filtering in curved 2D TI

Quantum spin Hall (QSH) system, two-dimensional (2D) TI, can exhibit exotic spin transport phenomena, mediated by its topologically protected edge channels[5, 6, 12, 13, 55, 59]. It has the advantage of being able to implement efficient generation and detection of pure spin current, which is one of the key challenges of spintronics. Especially, a transverse edge pure spin current can be generated under a four-terminal device setting[5, 55]. For a conventional flat QSH insulator, there are two basic properties, time-reversal symmetry (TRS) and spin conservation, which are of special interest. TRS renders the edge states of a QSH insulator topologically protected to transport robust spin current without elastic back-scattering from non-magnetic impurities. However, spin conservation mandates that there is no net spin current under a two-terminal device setting in a QSH system. Therefore, discovering new mechanism to control the spin current and/or transverse pure spin current in a QSH system is of great importance for spintronics devices. The original proposal to exploit the pure spin current in the QSH system has been demonstrated via bending strain engineering[60-63]. In layered materials, curvature or local strains are believed to affect the transport, magnetic, and spin relaxation properties[64-67]. Because the helicity of edge states should not be changed by the deformation, the rotation of orbitals by the bending strain leads to spin rotation[61]. Fig. 2 shows schematics of the adiabatic manipulation of counter-propagating spins along the edge of a curved QSH layer. For the flat QSH layer ($\theta_e = 0^\circ$), there exist both clockwise and counterclockwise edge channels, whose direction was determined by the spin orientation (either up or down) of the occupying electrons. For the curved QSH system ($\theta_e > 0^\circ$), curvature does not remove TRS, and spin/charge currents with opposite polarity still propagates in opposite directions along the edges, which is also reflected by the unchanged edge band structures. However, bending changes the directions of orbital angular momenta, which in turn changes the spin directions subject to the spin-momentum locking property.

Spins are no longer conserved along the edges, which is expected to modify non-equilibrium spin transport properties in curved QSH systems under a bias. Specifically, edge spin rotation is achieved by creating spin y (S_y) component in addition to S_z. At two opposite edges of a QSH ribbon, the S_z components are antiparallel (pointing in the opposite directions at opposite edges) but the S_y components are parallel (point in the same directions at opposite edges) to each other along the same direction of charge current. Consequently, a conventional (flat) QSH system conducts only charge current but not spin current under a two-terminal device setting because only S_z component exists, while a curved QSH insulator can conduct both charge current and spin current arising from the emergence of S_y component.

Based on the same physical mechanism, curvature can also modify the transverse pure spin current of QSH systems. More generally, using the Landauer-Buttiker framework[68], a comparison can be made between the charge and spin transport properties of curved QSH devices and those of conventional (flat) QSH devices in both two- and four-terminal device settings. In a two-terminal geometry [Fig. 2(d)-(f), upper panel], we expect a ballistic two terminal charge conductance (I) with conductance unit $I_0 = (\frac{e^2}{h})V$ for all three cases. While the spin current (I^s) for the curved QSH device is significantly different from the flat QSH device that conducts only charge current. The spin current varies from 0 to $(\frac{e}{2\pi})V$ according to the bending angle. A curved QSH device can effectively work as a topological half-metal for spin injection, that is, it transports topologically protected completely spin-polarized charge current, and the density of spin current can be tuned by the curvature. With four terminals setup, the flat QSH device conducts a longitudinal charge current (I_l) and a transverse pure spin current (I_t^s) [Fig. 2(d), lower panel], while the curved QSH device with $0<\theta_e<180°$ [Fig. 2(e), lower panel] conducts both longitudinal charge current $(I_l = I_0)$ and spin current $(I_l^s < I_0^s)$ (contributed by S_y component), as well as a transverse pure spin current $I_t^s < I_0^s$ (contributed by S_z component). Interestingly, I_t^s (I_l^s) continues to decrease (increase) with increasing θ_e subject to the conservation of total spin, $\boldsymbol{S}=\boldsymbol{S}_y+\boldsymbol{S}_z$, and finally I_t^s vanishes at $\theta_e=180°$ [Fig. 2(f), lower panel].

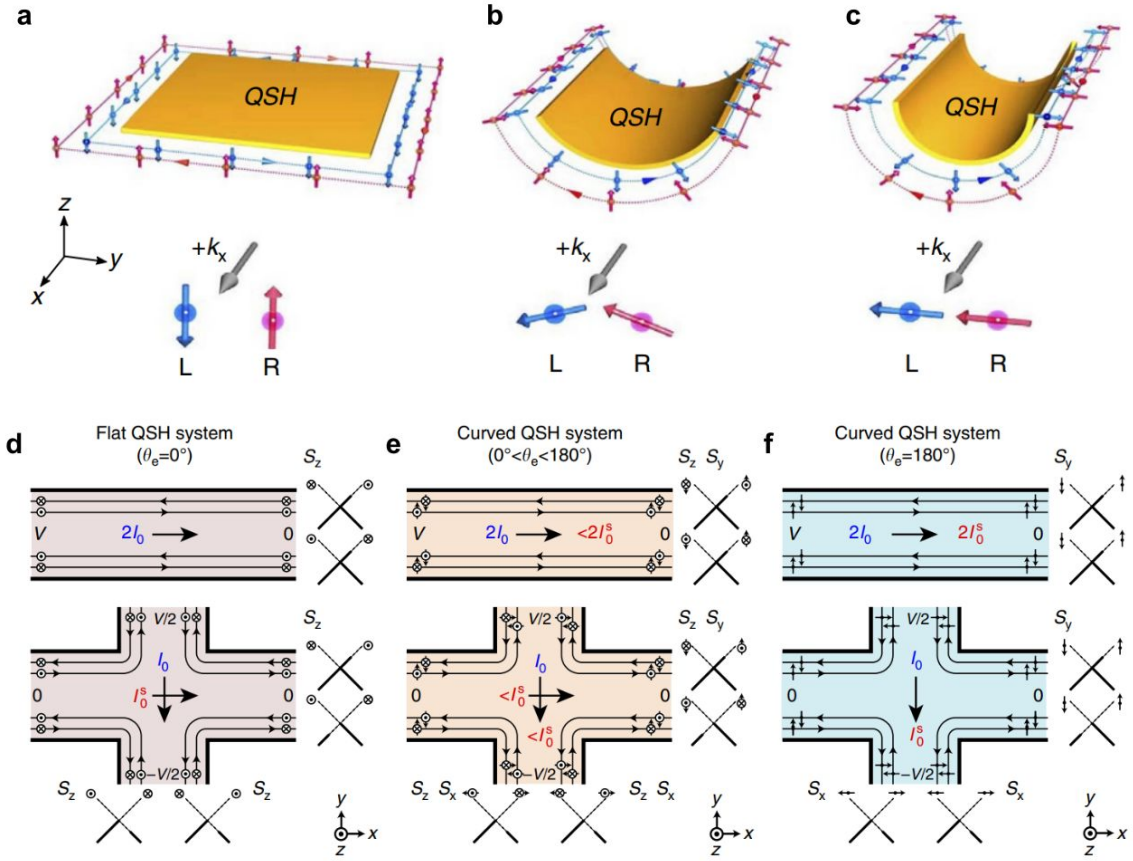

Fig. 2 (a)-(c) Schematic diagrams of spin current and charge current flowing along the edges as the bending angle θ_e increases from 0˚ to 180˚. A pair of edge states counter propagate along all four edges subject to TRS. The spins rotate adiabatically along the curved edges. (d)-(f) Comparison of two-terminal and four-terminal measurement geometries for a flat QSH system(θ_e=0˚), curved QSH system(0˚<θ_e<180˚), and curved QSH system (θ_e=180˚), respectively. The arrows indicate the charge current (I) (blue sign) and spin current (I^s) (red sign) and their flow directions. The unit of I and I^s are $I_0 = (\frac{e^2}{h})V$ and $I_0^s = (\frac{e}{4\pi})V$, respectively. The diagrams to the right and bottom indicate population of the edge states. Reprinted with permission from [61], Copyright 2017 Nature Publishing Group.

A practical approach to realize curved QSH systems is nanomechanical architecture of strained nanofilms, which has been proven a powerful method to fabricate nanomembranes, nanotubes, partial or half nanotubes, and nanocoils[69-71]. The general process of nanomechanical architecture proceeds with growth of strained nanofilms on a sacrificial substrate followed by patterning and release (through removal of the sacrificial substrate) of the nanofilms, which will roll-up into different tubular shapes as pre-designed by strain engineering. As a realizable curved QSH system, one promising example is a Bi(111) single layer with a puckered honeycomb lattice [Fig. 3(a)]. The Bi(111) single layer has been predicted and confirmed a QSH insulator with a large bulk gap and odd number of helical

edge states[72-76]. The concept of spin control through the bending strain can be applied to the Bi(111) single layer[60]. Fig. 3(b) shows schematics of deformation of zigzag Bi(111) nanoribbons and subsequent spin orientation in the edge states. The helical Dirac cone of edge states persists even when the nanoribbon is bent. The orbital rotation by the bending strain leads to the spin rotation to preserve the helicity. When both edges are bent parallel, both edges have the same spin direction, providing channels for spin-polarized currents. In order to achieve mechanical deformation in Bi(111) single layer, one can consider a contact-induced exfoliation of Bi(111) single layer [Fig. 3(c)]. Because the interlayer coupling is about 10 times weaker than the intralayer covalent bonding, once a gentle contact is made on the appropriate surface orientation, retracing the tip can peel off a single layer and bend it in the desired direction[77].

In addition to Bi(111) single layer, there are other curved QSH systems with self-bending[78], such as As-graphane[62] and Bi/Cl/SiGe(111) surface[61]. The As-graphane with As deposition on graphene with honeycomb H vacancies has been predicted as a new QSH insulator with a nontrivial gap ~83 meV [Fig. 3(d)]. Because of a large tensile surface stress in the As-graphane system (about 0.32 eV/Å^2), As-graphane nanoribbons will self-bend toward the graphane side [Fig. 3(e)]. After full relaxation, the As-graphane nanoribbon bends to the graphene side with a curved angle (the central angle of the curved nanoribbon) ~72˚. The naturally curved As-graphane nanoribbons then exhibit unique spin-filtered transport properties, distinctively different from the flat ones. In terms of feasibility, the surface-based QSH system[14, 79-82] has an advantage in its curved structure. It has been predicted that a surface based QSH state forms in a hexagonal Bi overlayer deposited in the halogenated Si/Ge(111) surface, that is, Bi/H(Cl)/SiGe(111). If one grows a ultrathin SiGe(111) film on a sacrificial SiO_2 substrate before Cl adsorption and Bi deposition, then the resulting Bi/H(Cl)/Si/Ge(111) nanofilm is readily subject to the nanomechanical architectural process[71], sell-rolling into a tubular shape including a partial cylinder type. Fig. 3(f) shows the atomic structure of Bi/Cl/SiGe(111) nanofilm and its self-curved nanoribbon structure. The calculated self-bending curvature of Bi/Cl/SiGe(111) is 0.0136 nm^{-1}, which satisfies the conditions for generating spin-rectified current with a configuration of parallel edges. Furthermore, a parallel process[83] that can facilitate mass production of identical partial cylindrical QSH arrays [Fig. 3(g) and (h)], which will function ideally as a robust spin injector device with high spin current density. The proposed a concept of bending strain engineering of spin transport in QSH systems, which is generally applicable to all QSH materials and especially suited for flexible atomic 2D QSH layers or surface-based QSH states on or inside a thin film.

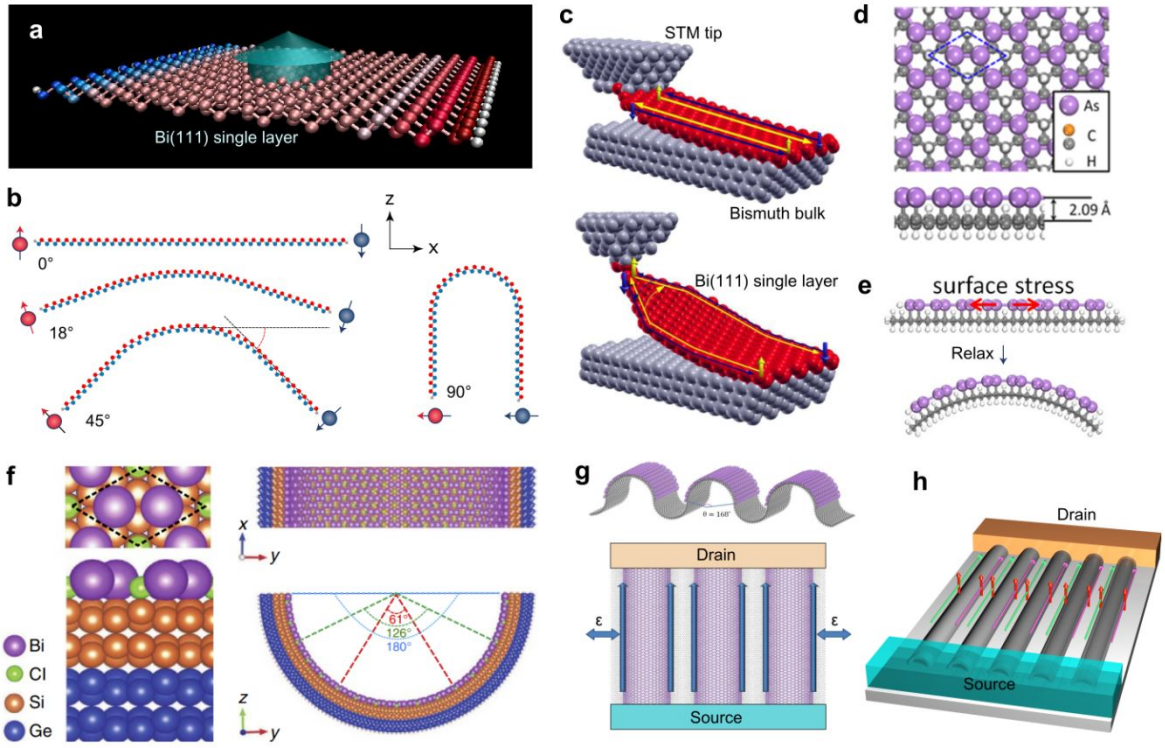

Fig. 3 (a) 2D topological Bi(111) single layer nanoribbon. (b) Cross-sectional view of curved Bi single layer nanoribbon. Reprinted with permission from [60], Copyright 2016 Royal Society of Chemistry. (c) The process of exfoliation of a Bi(111) single layer (red) after contact with the STM tip. One helical edge channel is represented. Reprinted with permission from [77], Copyright 2013 American Physical Society. (d) Atomic structure of As decorated graphane. (e) Side view of schematic configurations for the curving process of zigzag As-graphane nanoribbon. Reprinted with permission from [62], Copyright 2017 American Chemical Society. (f) Top and side views of a flat Bi/Cl/SiGe(111) surface and self-bent structure of a Bi/Cl/SiGe(111) surface, respectively. Reprinted with permission from [61], Copyright 2017 Nature Publishing Group. (g) Atomic structure of the naturally curved As-graphene nanoribbon arrays and its schematic design of a spin injector. (h) A proposed spin injector device concept: mass production of self-rolled up QSH nanofilms on a substrate produced by the concept of nanomechanical architecture process, connected with electrodes.

2.2 Control and manipulation of spin current in the TI/ferromagnet heterostructure

Efficient control and manipulation of spin degrees of freedom without a magnetic field is one of the challenges in developing spintronic devices[84, 85]. Taking inspiration from ordinary ferromagnetic heterostructures, proximity coupling has also been used for TI materials to achieve magnetic order, and thus enable the observation of topological phenomena with thermal stability[57, 86-89]. The coupling between the topologically protected surface states and the local magnetic moments can provide more interesting physics at the interface. In addition, the proximity coupling can break the time-reversal symmetry (TRS) while maintaining the TI surface free from impurities or lattice defects, overcoming the problem of large Dirac-mass disorder.

The nontrivial metallic Dirac band on the surface of a 3D TI, which is protected by the bulk topology order is the main characteristic feature. By introducing magnetism to a TI, either by magnetic impurity[90, 91] or by proximity coupling to a ferromagnet (FM)[92], TRS can be broken. The breaking of TRS induces a band gap in the Dirac surface states [Fig. 4(a)]. For the design of the next-generation spintronic devices, it is crucial to find efficient ways to magnetize their topological surface states (TSSs) while maintaining their topological features. The magnetized TIs by doping magnetic atoms has been realized in Fe-[91], Cr-[93] or V-doped[94] $(Bi, Sb)_2Te_3$ thin films. There also have been theoretical studies of the effect of magnetic atomic impurities on the topological properties[95-98]. Magnetic impurities in the bulk can lead to a small gap opening at the Dirac point. It was shown that magnetic Fe atoms on the Bi_2Se_3 surface act as strong Coulomb and magnetic scattering centers, which lead to the creation of odd multiples of Dirac fermions, and that magnetic interaction breaks TRS in the presence of band hybridizations[91]. On the other hand, a promising alternative route to magnetize TSSs is the ferromagnet (FM) and TI heterostructure via magnetic proximity effect. This approach provides a spatially uniform magnetization of TSSs and the absence of the dopant-induced scattering. Recently, many theoretical studies have been conducted to find suitable magnetic materials and to understand the physical mechanism occurring at the FM/TI interface[99-104]. Among them, 2D van der Waals ferromagnetic monolayer such as CrI_3 offers an optimal way to magnetize the TSSs [Fig. 4(b)]. The calculated band structure of $CrI_3/Bi_3Se_3/CrI_3$ shows the gapped Dirac cone of TSSs and lifted spin degeneracies indicating that the TSSs of Bi_2Se_3 are magnetized by the CrI_3[104].

In light of the above two approaches, different magnetic TI structures have been studied to probe the spin-orbit torque (SOT)-induced magnetization switching. As the first approach, the magnetization switching in the TI/Cr-doped TI heterostructure is reported[88, 105]. The Cr-doped TI structure is an ideal platform to study the SOT because it gives very robust ferromagnetism at low temperature[106]. In the TI heterostructure, the Cr-doped TI magnetization can be successfully switched by scanning the longitudinal current and a giant SOT is generated by the current flowing through the heterostructure[88]. Furthermore, the current-induced SOT in Cr-doped TI systems can also be controlled by the gate electric field[105]. Fig. 4(d) shows a top-gated Hall bar structure made of Au(electrode)/Al_2O_3/Cr-doped TI/GaAs(substrate). The top gate voltage can effectively tune the carrier density at the Al_2O_3/Cr-doped TI interface, and consequently the net SOT in the Cr-doped TI layer can be modulated. The SOT strength modulated by a factor of four by gate tuning within the accessible voltage range, which is 1-2 orders of magnitude larger than that reported in metal/ferromagnet heterostructures[107-109]. Furthermore, it is demonstrated that the magnetization switched by scanning gate voltage with constant current and in-plane magnetic field [Fig. 4(e)]. The gate voltage enabled switching points towards devices applications such as electric field controlled magnetic memories that are compatible with modern field-effect semiconductor technologies. Secondly, SOT-driven magnetization switching also has been demonstrated in FM/TI based structure, where the spin current generated by the strong SOC in TIs exerts a spin torque to the adjacent FM and thus switches the magnetization with a current[57, 110-113]. In particular, Ref. [113] demonstrated a TI-driven SOT-magnetic random-access memory (NRAM) cell with a state-of-the-art tunneling magnetoresistance (TMR)

ratio102% and an ultralow switching current density at room temperature. Fig. 4(f) show the 3-terminal SOT device of TI-magnetic tunnel junction (MTJ), the writing current is applied between terminal 1 (T1) and T2, where the spin-polarized current in TSSs is employed to provide the SOT and switch the magnetization of the free-layer (B-CoFeB) of the MTJ. For reading, a small vertical current between T1 and T3 is applied to pass through the tunneling barrier MgO, where the tunneling resistance strongly depends on the magnetization orientation between the free-layer (B-CoFeB) and the fixed-layer (T-CoFeB): low resistance for the parallel state ("0" state) and high resistance for the antiparallel state ("1" state), respectively, i.e., the TMR effect. From the cross-sectional scanning transmission electron microscopy results, we see the layer-by-layer (i.e., van der Waals) structure of the TI [$(BiSb)_2Te_3$] and the clear interface between TI and MTJ [Fig. 4(g)]. Fig. 4(h) shows the tunneling resistance R and the TMR ratio as a function of the magnetic field H at room temperature, where a TMR ratio of 102% indicates the energy consumption is significantly reduced.

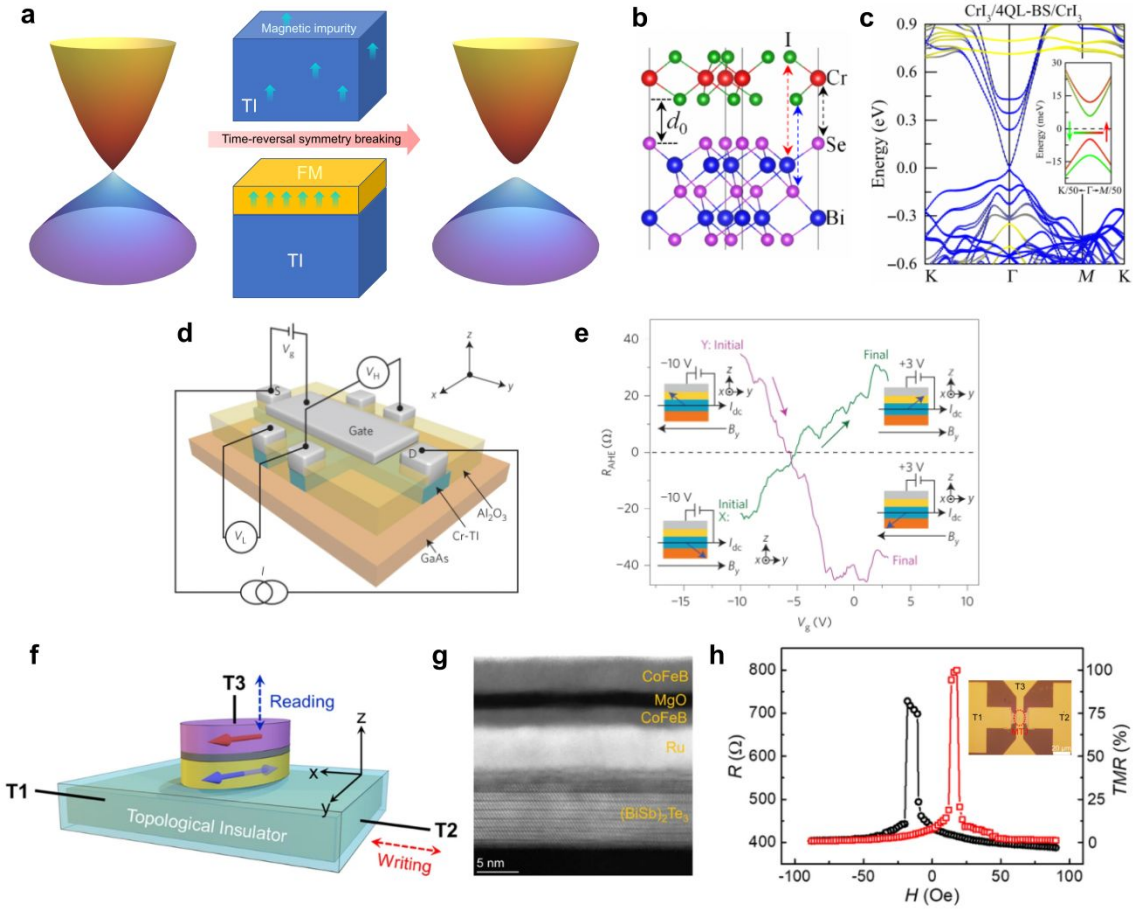

Fig. 4 (a) Linearly spin-polarized Dirac band of TSS and gapped TSS by breaking time-reversal symmetry. The broken time-reversal symmetry induced by magnetic impurity doping or proximity coupling with a ferromagnet (FM). (b) Side view of $CrI_3/Bi_2Se_3/CrI_3$ heterostructure. (c) Band structure of CrI_3/4QL-Bi_2Se_3/CrI_3. Colors in the main panels indicate the contributions from Bi_2Se_3

(blue) and CrI_3 (yellow). Colors in inset indicate the spin projections. Reprinted with permission from [104], Copyright 2019 American Association for the Advancement of Science. (d) Schematic of the Hall bar structure with the Al_2O_3(20 nm)/Cr-TI(7 nm)/GaAs(substrate) stack. Standard four-point measurement set-up is displayed. A gate voltage of V_g can be applied between the top gate and the source contact. (e) Magnetization switching induced by scanning V_g in the presence of constant B_y and I_{dc} for X: ($I_{dc} = 20\,\mu$A, $B_y = 0.1$ T) and Y: ($I_{dc} = 20\,\mu$A, By $= -0.1$ T). Insets show the corresponding initial and final magnetization configurations. Reprinted with permission from [105], Copyright 2016 Nature Publishing Group. (f) Schematic of the 3-terminal SOT-MRAM cell with a TI. The writing current applied between T1 and T2 is used to switch the MTJ between TI and T3. In the T1, the spin-momentum locking of the surface states provides a giant SOT. (g) Cross-sectional scanning transmission electron microscopy image shows the layer-by-layer structure of the TI/FM and the clear interface. (h) Tunneling resistance R and TMR ratio as a function of the magnetic field, where the 102% TMR ratio indicates the high quality of MTJ. Inset shows the patterned SOT-MRAM device. Reprinted with permission from [113], Copyright 2021 Nature Publishing Group.

2.3 Topological dislocation induced unique spin texture with high spin coherency

The structural, mechanical, and electronic properties of dislocations have been intensively studied for decades [114-116]. They fall into three categories, i.e., edge, mixed, and screw type[114]. In general, dislocations are considered to have a negative impact on materials properties and functionalities. For example, formation of dislocation is the leading mechanism for growth instability of coherent thin films. Dislocations may create scattering centers[115, 116] to lower carrier mobility, cause current leakage and act as in-gap deep-level carrier recombination centers[117, 118]. Therefore, much research effort in the past has been devoted to alleviating dislocations in semiconductors[119]. However, using the unique structure of dislocation (topological singularities and line defects) and the SOC effect, the ordinarily harmful dislocation turns into a beneficial unit for spintronic devices[120-124]. In a crystalline solid, the motion of an electron is inevitably coupled with its spin orientation through the SOC effect. Hence, discovering new forms of the SOC effect and topological behavior in the dislocations that provide more effective means to manipulate spin transport properties is not only of fundamental interest but also critical to the development of spintronics devices.

The extrinsic SOC effect in a crystal requires breaking of inversion symmetry, which commonly occurs on surfaces or interfaces as manifested by the 2D Rashba[125] and Dresselhaus SOC[126] (RD-SOC) effects [Fig. 5(a)]. For the pure Rashba SOC, the spin is always orthogonal to the **k** vector. For the Dresselhaus SOC, the spin can be either parallel or orthogonal to the **k** vector. In the case of equal contribution of Rashba and Dresselhaus effect, the spin-orbit field becomes unidirectional, i.e., the persistent spin texture[127, 128]. On the other hand, the SOC in a screw dislocation (SD) is 1D in nature and exists in bulk materials, so it goes much beyond the conventional 2D RD-SOC effect. In Ref. [123], it demonstrated the key features of the coherent 1D SD-SOC effect and its main difference from a conventional 2D RD-SOC effect [Fig. 5(b)]. For the newly discovered 1D SD-SOC [Figs. 5(b)], spins only rotate in one quadrant with an angle changing from 0 to $\pi/2$. Consequently, the 1D SD-SOC will exhibit a significant higher degree of spin coherency because the spins are constrained to vary within a much narrower range of angles. Furthermore, similar to the persistent spin

texture in 2D system, an ideal spin texture can be achieved in 1D SD-SOC, albeit be available intrinsically in a single material.

This new type of SOC was confirmed on three representative semiconductors: Ge, GaAs, and SiC[123]. For each material, a model for the single dislocation defect was constructed [Fig. 5(c)]. The crystal field around the defect can be broken into two components—one Rashba-like, the other Dresselhaus-like. In addition, the ratio of these two components depends on the compound's ionicity, which is a measure of how ionic the atomic bonds are. Purely Dresselhaus-like SOC occurs in the compound with the weakest ionicity, Ge, while the Rashba-like contribution dominates in the compound with the strongest ionicity, GaAs. Interestingly, the two contributions are equal in SiC, whose ionicity is between that of Ge and GaAs. The Rashba and Dresselhaus contributions rotate spins in opposite directions, so having an equal contribution of the two produces spins with a fixed orientation [Fig. 5(d)]. Thus, the SD in those compound semiconductors with medium iconicity, like SiC, may be used effectively for suppressing spin relaxation in spintronics devices.

The 1D SD-SOC character in 3D bulk materials can be extended to 1D line defects of 2D systems[124]. 2D materials with atomic thickness and high exposure of surface atoms allow for easy regulation of properties by means of defect engineering[129]. Especially, monolayer transition metal dichalcogenides MX_2 (M = Mo, W; and X = S, Se) suitable for three critical reasons: (1) controllable defects engineering, (2) a moderate band gap (~1-2 eV) providing the possibility to create ideal SOC states free of interference from bulk states, (3) large SOC strength enabling effective manipulation of spin states. In Ref. [124], the proposed chalcogen vacancy line defects are oriented along the armchair direction of MX_2, and the two parallel aligned line defects are separated by a single atomic line, as shown in Fig. 5(e). The spin-projected conduction bands of the double line defects engineered WS_2 where are expectation value of spin x component is clearly shown in Fig 5(f). These in-gap defect states are completely isolated from other bulk bands. Spin components of S_y and S_z are both zero, and the only nonzero spin component is S_x along the entire path of Γ-X. This suggests that the defect states have uniaxial spin polarizations oriented along the x direction, which forms exactly the desired unidirectional SO field. Interestingly, when the relative positions of double line defects change, spin polarization of the defects states changes from x to y direction. The emerging unidirectional SO field is subject to both the structural symmetry and 1D nature of the line defects. The orientation of the SO field can be effectively tuned by altering the line defect spatial distribution.

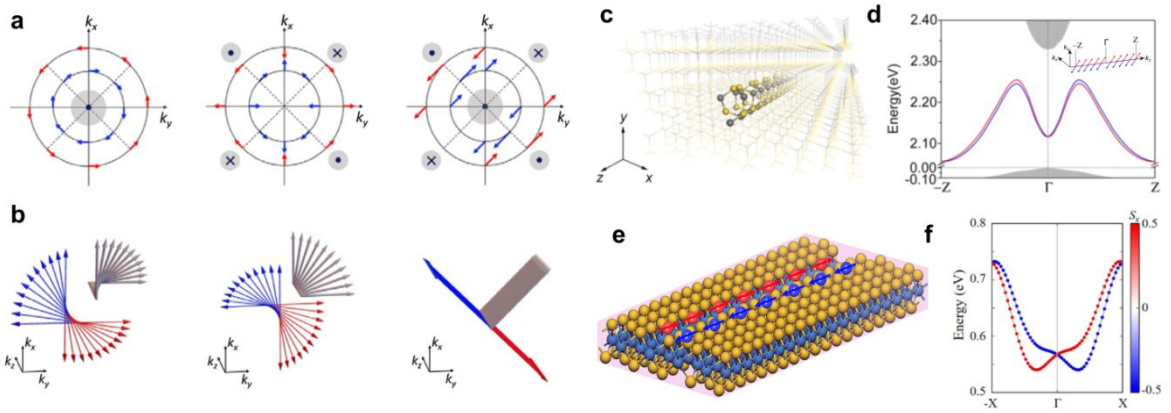

Fig. 5 (a) The orientations of the effective electrical field (light gray shaded circle) and spins (red and blue arrows) for the conventional Rashba SOC effect at surfaces or interfaces, for the linear Dresselhaus effect in an asymmetry QW or a strained zinc-blende film and combined effect of Rashba and Dresselhaus effect, respectively. (b) The orientations of the effective electrical field (gray arrows) and spins (red and blue arrows) for the 1D SD-SOC effect as found in Ge, GaAs and SiC, respectively. (c) The atomic structure of a SD in bulk SiC. (d) Band structure of a SD in SiC with SOC effect. The red and blue lines represent SD-SOC bands with different spin projections. Inset shows the spin textures of SD-SOC bands. The red and blue arrows show orientations of two spin projections. Reprinted with permission from [123], Copyright 2018 American Physical Society. (e) Atomic structure of WS_2 with two parallel aligned S vacancy line defects. (f) Spin-projected conduction bands of line defects engineered WS_2. Reprinted with permission from [124], Copyright 2019 American Chemical Society.

2.4 Persistent spin texture in 2D non-centrosymmetric materials

Rich and exotic electronic properties may arise through symmetry breaking in 2D materials, which have recently attracted much attention for both fundamental interests and novel spintronic device concepts. The SOC in inversion asymmetric system has been an important factor in spintronics since the development of the Datta-Das spin field-effect transistor[130, 131], which induces the coherent spin precession governed by the Rashba SOC [Fig. 6(a)]. However, the Rashba SOC is rarely compatible with long spin lifetimes because it breaks the spin rotational symmetry and suffers from fast spin decoherence in a diffusive transport regime[128]. Thus, acquiring effective electrical spin manipulation while preserving the long spin lifetime has been elusive. As an exceptional example, in the case of PST [Fig. 6(b)], the spin-orbit field is unidirectional which results in a spatially periodic mode known as a persistent spin helix (PSH)[132] [Fig. 6(c)]. In addition, recent studies reported that the PSH feature is closely related to the topological characters, such as Berry curvature dipole, valleytronics, and nonlinear Hall effects[133, 134]. The PSH has spatial periodicity with the wave length l_{PSH} defined as the distance over which the spin direction repeats. The combined spin-orbit field is aligned in a uniaxial direction with SU(2) symmetry, which is robust against spin-independent scattering and renders the spin lifetime ultimately infinite[128] [Fig. 6(d)]. It has been demonstrated that the PSH states can be achieved in specific noncentrosymmetric bulk materials where the PSH state is enforced by the nonsymmorphic space group symmetry

of the crystal[135, 136]. However, these states survive only along certain high-symmetry paths in the Brillouin zone and are likely overwhelmed by other non-PSH states in the same energy window, which severely hamper their practical applications. Therefore, it is highly desirable to explore material platforms for realizing the PSH states.

The ideal target system for PSH states should simply possess a unidirectional, field-tunable, and large SOC. Specifically, atomically thin SnTe film, recently synthesized using molecular beam epitaxy, is the most promising material potentially capable of satisfying the criteria[137-139]. Fig. 6(e) shows the SnTe monolayer structure. The ions are arranged in two buckled layers with distortions inducing the spontaneous polarization along x, while the tiny anisotropy between the lattice constants a and b emerges as a natural signature of the ferroelectric phase. When the ferroelectric polarization is aligned along the x-axis, the electronic structure of the SnTe monolayer exhibits two valleys near points X and Y[139] [Fig. 6(f)]. In particular, the energy levels without the SOC are fourfold degenerate, while the SOC splits them into doublets over the entire Brillouin zone (BZ) except for the Γ-X line. Furthermore, these doublets split into singlets with eigenvalues of spin operator S_z, indicating the PST (anti-)aligned in the out-of plane direction. The spin texture of topmost valence band clearly shows unidirectional PST aligned along the z-direction. The estimated l_{PSH} of SnTe monolayer falls within the range 8.8-18.3 nm which improves the suitability for use in nano-size spin transistors by handling the rapid but coherent spin precession[138]. Another promising material platform is a buckled Bi(110) monolayer[133, 134]. A notable structural feature of Bi(110) monolayer is the finite out-of-plane buckling, resulting from the vertical shift of the two centered Bi atoms [Fig. 6(g)]. The structural distortion creates internal in-plane ferroelectricity with inversion asymmetry. Similar to SnTe monolayer, the in-plane ferroelectricity induces a momentum-independent spin orientation. As shown in Fig. 6(h), a unidirectional spin splitting is observed along the k_y-direction. The glide mirror symmetry allows the z spin component only in each spin-polarized band. Ref. [134] further shows that such novel electronic properties can be secured in a Bi(110) film grown on a proper substrate such as a Bi(110)/$NbSe_2$ heterostructure [Fig. 6(i)]. Furthermore, Bi(110)/$NbSe_2$ heterostructure provides a promising platform for realizing a sizable Berry curvature dipole and nonlinear Hall effect which fundamentally related with PST.

Considering the non-volatile control over the ferroelectricity, SnTe and Bi(110) thin films could enable novel multi-functional spin transistors[138]. As a simple sketch for a device application, a spin-valve-like experimental setup composed of ferromagnetic electrodes and a noncentrosymmetric thin film as a transport channel could facilitate two switching modes by employing a ferroelectric-coupled PSH. Ferromagnetic metal leads at both ends have in-plane and orthogonal spin orientations, and the ferroelectric polarization in the monolayer channel aligns perpendicular to the transport direction. Due to the orthogonal spin configurations between the ferromagnetic source and drain electrodes, the electron spin at the end of the monolayer channel is either parallel or antiparallel to the spin orientation of the drain, leading to an on- or off-state, respectively. The on-off switching could be controlled by flipping either the electric polarization of the monolayer channel [Fig. 6(j)] or the magnetic polarization of the ferromagnetic electrodes [Fig. 6(k)]. Combined with the charge switching mechanism along the polarization direction, we can design the multi-functional cross-shaped

charge-spin transistor sketched in Fig. 6(l).

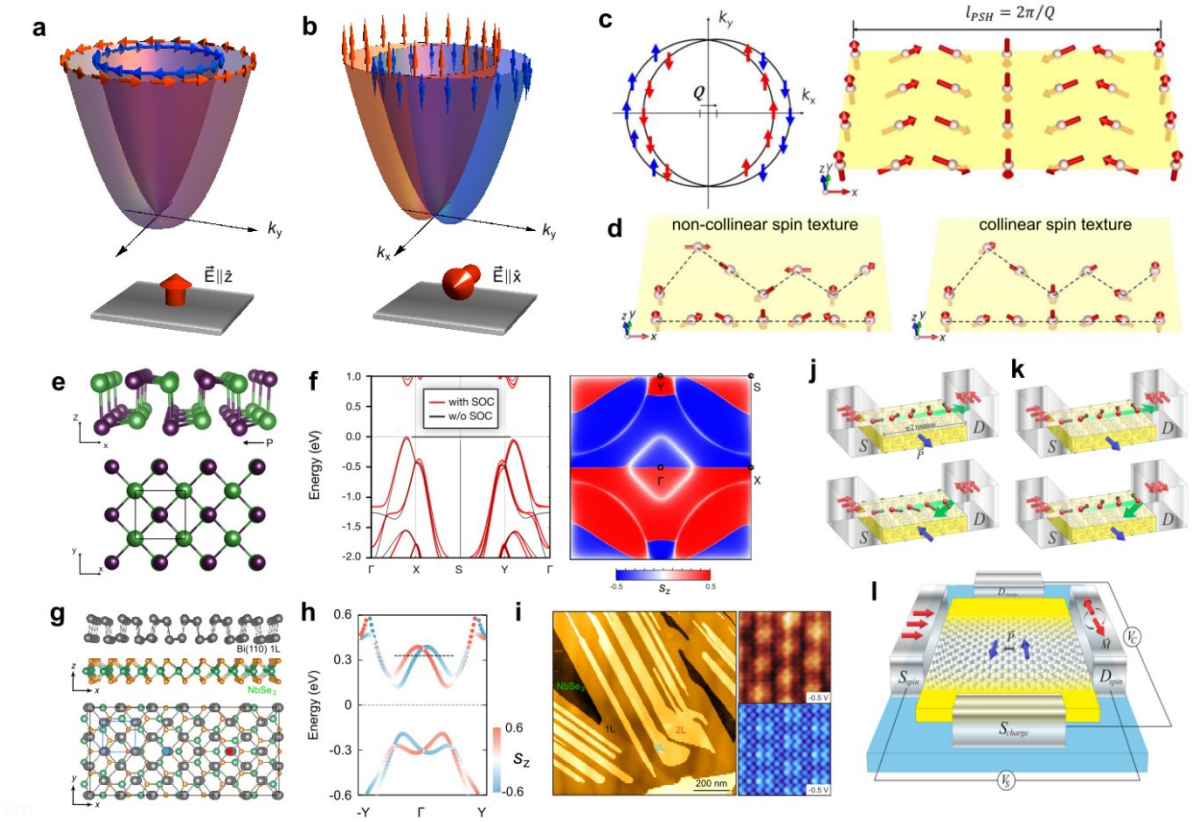

Fig. 6 (a),(b) The conventional Rashba and PST spin configurations appear under the out-of-plane (*z*-direction) and in-plane (*x*-direction) electric field, respectively. (c) The unidirectional spin-split Fermi surface with the long-lived persistent spin helix mode. The spheres (arrows) represent electrons (spin directions). l_{PSH} denotes the persistent spin helix wavelength. (d) Schematic images of spin propagation across the channel with non-collinear spin texture and the colinear spin texture. Reprinted with permission from [136], Copyright 2021 IOP Publishing. (e) Top and side view of SnTe monolayer. (f) Band structure of SnTe monolayer along the high-symmetry and the spin polarization (S_z component) of topmost valence band over the entire BZ. Reprinted with permission from [139], Copyright 2020 IOP Publishing. (g) Atomic structure of Bi(110)/NbSe2 heterostucture. (h) Spin resolved band structure of the puckered Bi(110) monolayer. (i) STM morphology of Bi(110)/NbSe2. Right panels show the atomically resolved STM image and simulated STM image. Reprinted with permission from [134], Copyright 2021 American Chemical Society. Non-volatile (j) electric and (k) magnetic on-off switching mechanisms in the spin-valve structure. (l) A multi-functional cross-shaped charge-spin transistor. Reprinted with permission from [138], Copyright 2020 AIP Publishing.

3. Topological electronic devices

Considering the most prominent property of topological materials[140], i.e., TSSs with spin-momentum locking, they are touted as promising electronic transport materials with potentially higher transport efficiency and lower power consumption. In this section, we will review recent studies on the application of topological materials in electronic devices. We

start from the usage of TIs in traditional field-effect transistor (FET), which are termed as topological FET (TFET), and briefly review proposals of using different categories of topological materials for TFET based on topological phase transitions. Then, the application of topological materials in another fundamental electronic device building block, p-n junction, in both in-plane and vertical configurations are reviewed. Furthermore, some less mentioned applications of topological materials in electronic devices will be briefly outlined.

3.1 Topological field-effect transistor

Field-effect transistors have built the foundation for modern electronic devices that was believed to continually follow Moore's Law to achieve faster and more powerful digital information processing ability. One key contribution to such amazing achievement is the continued miniaturization of device components, such as complementary metal-oxide-semiconductor (CMOS) unit, which, however, may have eventually reached its limit that prevent from further development. To meet the further future demand on performance improvement, one alternative pathway for advancement is to decrease the power consumption and find novel materials that are less affected by the confinement effect. There are several promising attempts in term of architecture revolution, such as vertical transport FET[141], gate-all-around transistors[142], and crossbar-based computing architectures[143], et. al. These advancements have gradually matured and adopted in the next generation of electronic devices[141]. On the other hand, extensive research efforts have been made in discovering new materials to replace the conventional semiconductors, which would lead to a more disruptive technology advancement. Several most studied families of materials include but not limited to organic semiconductors[144-146], ferroelectric semiconductors[147-149], two-dimensional materials[150-152], and topological materials[153-155], which however all have their pros and cons. There are already several comprehensive reviews available about some of these novel functional materials for applications in FET[156-158], here we will focus on the emerging topological materials studied in TFET.

As mentioned in the introduction, a number of different categories of topological materials have been proposed theoretically and discovered experimentally, including insulating, metallic and semi-metallic materials of different dimensionality[7, 9, 15, 16, 55, 159-166]. Among them, TIs that have bulk insulating states and spin-momentum locked edge/surface states are considered as the most promising candidates in TFET at the early stage of the study[7, 140, 159, 160]. This is mainly because it is believed that the bulk insulating state can adopt conventional on-off switching mechanism, and the additional TSS without backscattering and thus no energy dissipation may facilitate more efficient charge transport and lower power consumption.

One well-studied case is based on 3D TIs, e.g., Bi_2Se_3 and other binary sesquichalcogenides[16,

[167-169], which are directly employed as a channel material in FET[170-174]. There are several key challenges that have been encountered and yet to be fully resolved, e.g., (i) feasible tuning of carrier density of TIs through electric field; (ii) relatively high bulk conductivity compared to the TSS; (iii) high bulk carrier concentration caused switching difficulty between n- and p-type carriers; (iv) constrained operation temperature limited by relatively small band gaps of known TIs, etc.

Several potential solutions have been proposed and tested experimentally[170-174]. One of the initial studies based on Bi_2Se_3 thin film applied a dual gate configuration to achieve an independent-tuning of carrier density through either top or back gate, as shown in Fig. 7(a)[170]. Parallel bulk and surface state contributions to the total conductance were observed and an ambipolar conduction was demonstrated. To reduce the contribution of trivial bulk electrons to the conductivity, thin films were proposed for TFET devices to take advantage of the confinement effect[175]. With the decreasing film thickness, the bulk state moves away from the Fermi level, leading to substantially reduced bulk conductivity, as shown in Fig. 7(b)[176]. Bi_2Se_3 thin film with different thickness (3-14 nm) was studied, which showed successful electron depletion for both surface and bulk state through gate voltage control in TFET. Also an insulator state was observed when the thickness is reduced below 3.5 nm[175]. However, such insulating state is presumed to be caused by the coupling of the top and bottom surface state that destroys the topological feature and forms a conventional trivial insulator[177-179].

Another difficulty related to tuning the carrier type, which cannot be fully resolved by reducing the film thickness, is the residual charge carriers contributed by crystal defects or environmental doping. Suitable element doping is proposed to shift the Fermi level to conduction band edge and thus reduce the bulk carrier concentration, in order to realize successful switching between n- and p-type carriers through gate voltage control. Two feasible approaches had been successfully demonstrated experimentally, through either Ca doping[173] or forming ternary TIs $(Bi_xSb_{1-x})Te_3$ by composition tuning[174]. In general, many efforts have been made for the application of TFET, which however are constrained by the gap size of Bi_2Se_3, even though the gap size could increase through confinement effect. In addition, all the transport data show either parallel contribution from bulk and surface states of a TI or a completely insulating state induced by further decreasing the film thickness that destroys the TSS.

To solve the aforementioned issues, another proposal that relies on the electric-field-induced topological phase transition between normal insulator (NI) and TI has been brought up to serve as the foundation for the TFET, as shown in Fig. 7(c)[180, 181]. Specifically, the device is built using 2D van der Waal topological materials, e.g., transition metal dichalcogenides (TMD), which show tunable topological states through either vertical electric field and/or strain, shown in Fig. 8(a)[180]. A series of large-gap 2D TMD TI candidates have been studied theoretically, and a novel TFET was proposed by stacking TMD TIs with wide-gap NIs, as

shown in Fig. 7(c). Several advantages have been discussed, including easy switch between NI and TI, i.e., OFF and ON states; better control of the band gap through external electric field; multiple conduction channels through decoupled multiple-layer set up in the heterostructure; easier thickness control of the 2D materials to minimize devices size[180]. Instead of using the TI/NI state as the ON/OFF state, recently, a TFET based on tunable topological dislocation states with quantized conductance for both ON and OFF states was proposed[182], as shown in Fig. 7(d). In the proof-of-concept device, two topological screw dislocation states in three-dimensional TIs can be controlled separately by two local fields, which support two quantized conducting states ($2e^2/h$ and e^2/h) that effectively serve as ON and OFF states, respectively. As both ON and OFF states are topologically protected with quantized conductance, the TFET is rather robust, precise, and energy efficient, which may serve as a new framework for realizing high-fidelity topological quantum devices.

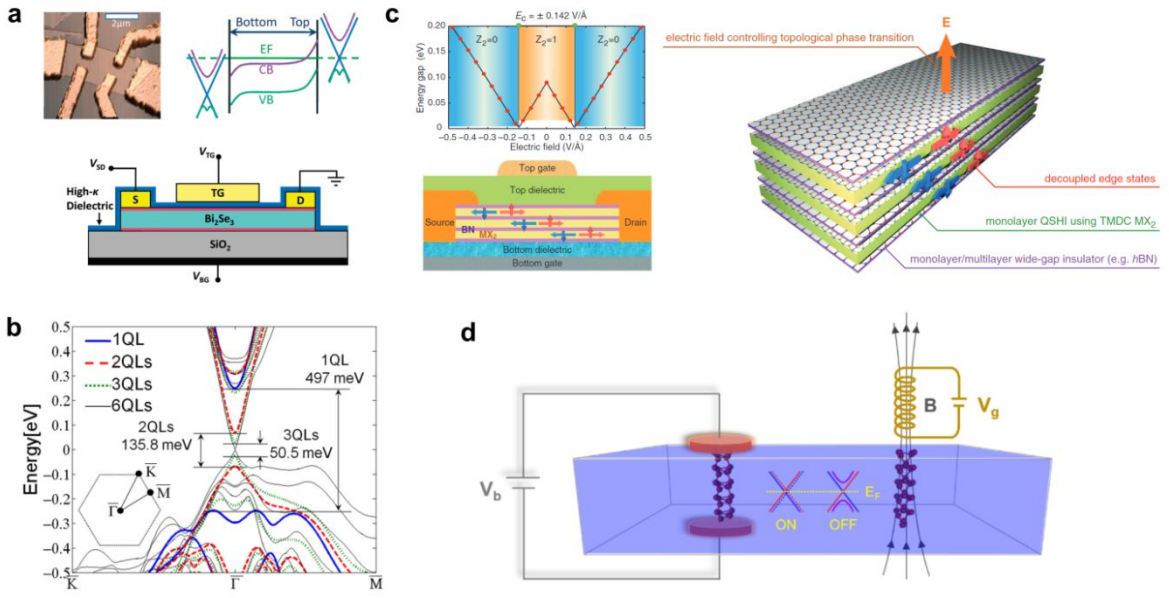

Fig. 7 (a) Topological field effect transistor based on TI Bi_2Se_3 with both top and bottom gate. Reprinted with permission from [170], Copyright 2010 Royal Society of Chemistry. (b) Evolution of the topological surface and bulk state of Bi_2Se_3 with different layer thickness. Reprinted with permission from [176], Copyright 2012 AIP Publishing. (c) Theoretically proposed TFET based on 2D topological materials with topological phase transition through vertical electric field. Reprinted with permission from [180], Copyright 2014 Science Publishing group. (d) Theoretically proposed high-fidelity TFET enabled by topological dislocation states, in which two local gates control the quantized ON and OFF states. Reprinted with permission from [182], Copyright 2023 American Physical Society.

Similarly, several different mechanisms for inducing topological phase transitions have been proposed for various topological materials. For example, topological phase transition in a

family of topological crystalline insulators, such as the one by applying an electric field perpendicular to the SnTe film, has been studied, as shown in Fig. 8(b), and a high on/off operation speed is expected[183]. Figure 8(c) shows strain modulation of topological states in a piezotronics transistors based on topological heterostructure HgTe/CdTe[184]. Also, one experiment demonstrated another interesting topological phase transition between topological semimetal, TI and trivial insulator in Na_3Bi system[185]. The bulk topological semimetal phase of Na_3Bi naturally transforms into a TI in a thin film of a few layers thick owing to confinement effect, which can be further tuned into a trivial NI through electric field, as summarized in Fig. 8(d)[185-187].

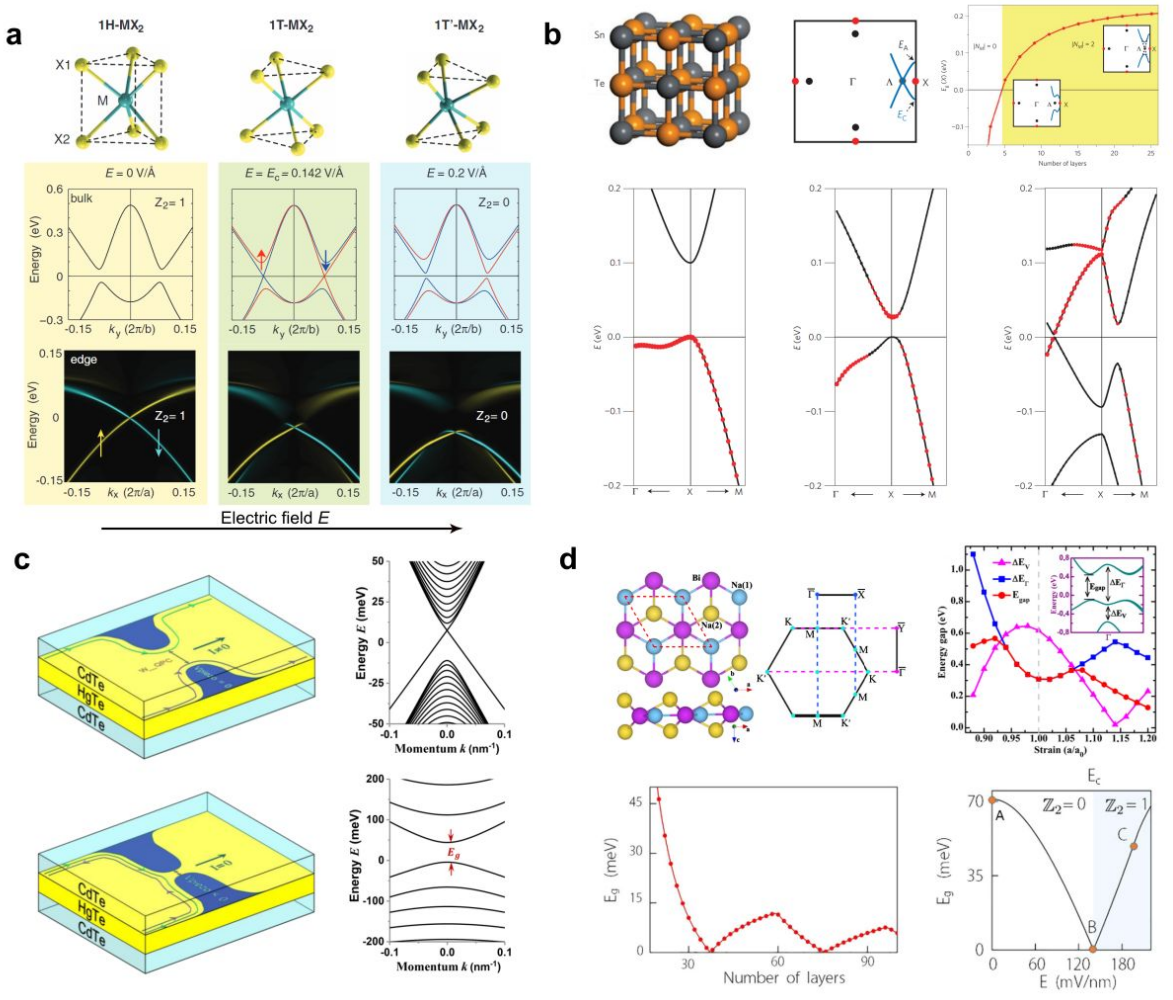

Fig. 8 (a) Topological phase transition of 2D TI, transition metal dichalcogenide, under perpendicular electric field. Reprinted with permission from [180], Copyright 2014 Science Publishing group. (b) Topological phase transition of topological crystalline insulator, SnTe, with different number of layers. Reprinted with permission from [183], Copyright 2014 Nature Publishing group. (c) Topological phase transition of topological heterostructure HgTe/CdTe. Reprinted with permission from [184], Copyright 2018 Royal Society of Chemistry. (d) Topological phase transition of Na_3Bi with different layer thickness under strain and electric field. Reprinted with permission from [186, 187], Copyright 2017 American Physical Society and 2015 Nature Publishing group.

To compare the performance between the newly proposed TFET and other theoretically proposed and experimentally well-developed FET technologies, two factors, i.e., switching delay and its associated switching energy, were studied for benchmarking[152, 181]. The results of comparison suggest that TFET may be able to compete with current high-performance CMOS technologies for its potentially low power consumption with similar switching speed. However, the application of TFETs remains challenging due to their generally large capacitance, and the early expectation of high mobility due to TSS remains elusive[152]. Better electric field control with suitable selection of topological materials is necessary to achieve new breakthrough that could potentially disrupt the current information processing technology.

3.2 Topological p-n junctions

Another fundamental building block of modern electronic devices is p-n junction, which consists of an interface between p-type and n-type semiconducting materials. Its unique feature of one-directional current flow makes it the key component for many electronic devices, such as diode, transistors, and integrated circuits. Similar structure can be created by stacking topological materials with electron and hole doping, which however does not serve the same purpose as traditional p-n junctions and possesses quite distinct properties. Unlike conventional p-n junction, where the junction is depleted of charge carriers that is non-conductive. The topological p-n junction is believed to form a standing wave state[188] at the interface due to the interference between the incident and reflected waves, which can further induce a gapless chiral edge state through a perpendicular magnetic field[189].

Though the application of topological p-n junction in electronic devices was not well justified, it does demonstrate several promising features for useful application in other aspects. For example, such p-n junction has been used to tune the chemical potential of the topological Dirac point[190]. This is realized in a vertical p-n junction with epitaxial Sb_2Te_3/Bi_2Te_3 heterostructure, as shown in Fig. 9(a), where the chemical potential is able to shift about 200 meV by simply changing the Sb_2Te_3 layer thickness from 25 to 6 quintuple layers. It provides one feasible pathway to study exotic quantum states related to Dirac points[190].

Motivated by the graphene p-n junction that shows angle-dependent transmission (chiral tunneling)[191], topological p-n junction is expected to show similar chiral tunneling behavior. Theoretical calculations show that ideal topological p-n junction indeed allows only the transmission of electrons with very small incident angle due to the chiral tunneling effect, as shown in Fig. 9(b)[192]. Moreover, those electrons all possess the same spin due to the spin-momentum locking. Such special transmission behavior makes topological p-n junction as a

promising spin filter that generates pure spin current. Because all the other electrons are reflected, it could also substantially reduce the charge current that helps to reduce power consumption[192]. Also, a very similar spin filtering phenomena (spin-dependent Mach–Zender interferometer) was proposed for the topological p-n junction around the same time[193]. Differently, an external perpendicular magnetic field is required to tune both the top and bottom surfaces into the quantum Hall regime to function as the spin filter through electronic gate control[193].

Along with the theoretical demonstration of the aforementioned intriguing phenomena, several proposals have been made experimentally, such as composition graded doping and electrostatic gating[189]. Beside the vertical topological p-n junction formed through epitaxial Sb_2Te_3/Bi_2Te_3 heterostructure[190], in-plane p-n junction has also been experimentally realized[194, 195]. Based on an n-type TI thin film, $Bi_{2-x}Sb_xTe_{3-y}Se_y$, half of the thin film is properly treated by organic acceptor molecules that transform into a p-type TI while the other half is untouched that remains n-type, which forms an in-plane topological p-n junction, as shown in Fig. 9(c). Through proper field control from both top and bottom gates, distinct transport behaviors were observed, confirming characteristic p-n junction features[194].

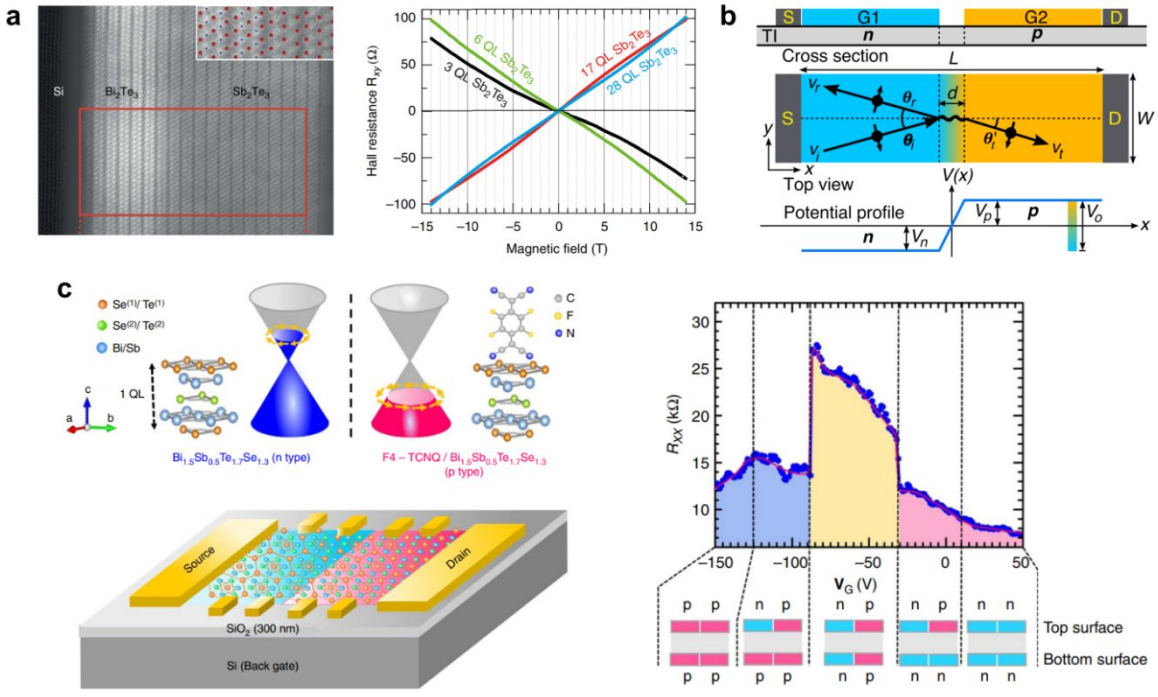

Fig. 9 (a) Vertical topological p-n junction built through epitaxial Sb_2Te_3/Bi_2Te_3 heterostructure that shows feasible control of chemical potential with different Sb_2Te_3 thickness. Reprinted with permission from [190], Copyright 2015 Nature Publishing group. (b) Chiral tunneling of topological p-n junction that forms an ideal spin-filter. Reprinted with permission from [192], Copyright 2015 American Physical Society. (c) Formation of in-plane topological p-n junction through half-film

molecular adsorption, that shows feasible electronic gate control. Reprinted with permission from [194], Copyright 2016 Nature Publishing group.

3.3 Other topological electronic applications

Beside the most fundamental application of topological materials in electronic devices, there are quite a few less known but still important aspects where topological materials could be useful. One is the interconnect of the CMOS devices, where the traditional metallic interconnect is severely limited by the finite size effect due to the fast increase of the resistivity and switching delay with the decreased size[196]. Considering the high mobility and lack of back-scattering feature, TIs could potentially serve as efficient interconnect materials. Theoretical modeling using Bi_2Se_3 as interconnect has been performed through real-space transport calculation, which however shows that the mobility becomes much lower than Cu interconnect due to strong acoustic phonon scattering at room temperature[196]. A larger-gap TI with weak acoustic phonon scattering is necessary for such application.

In addition, application of topological materials in Josephson bifurcation amplifier has been proposed to form a topological Josephson junction[197], which could help to understand the Majorana bound state and superconducting qubit-based quantum information processing technology. The devices based on Dirac and Weyl materials possess distinct characteristics and offer unique advantages in various applications[9]. The Dirac materials, characterized by their linear dispersion relation, exhibit massless quasi particles with high mobility. This property enables efficient charge transport making them promising for high-speed electronic devices and low-power consumption applications. Recently, FET chiral devices[198] are demonstrated with Dirac semimetal $PtSe_2$ showing the ON/OFF ratio of more than 10^3. On the other hand, Weyl semimetal exhibits a different type of behavior, with Weyl nodes acting as magnetic monopole-like sources or sinks of Berry flux. This gives rise to unique transport properties, including the chiral anomaly and the Fermi arc surface states. The existence of Weyl fermions opens up possibilities for high-mobility electronics and potential applications in quantum computing. With strong SOC and broken inversion symmetry, exotic spin textures enable a large spin Hall effect that can efficiently convert the charge into spin current in a type-II WTe_2 Weyl semimetal[199, 200]. While both Dirac and Weyl devices share similarities in terms of their topological nature, their distinct band structures and associated phenomena provide different applications. There is also another interesting field that uses non-Hermitian topological systems as novel high-precision sensors[201]. The key design principle is to couple the boundary conditions that define the non-Hermitian topological systems with those measurable physical quantities. Theoretical modeling founds these novel sensors show increasing sensitivity with the size of the device and high stability against perturbations[201].

4. Topological Optoelectronic devices

In this section, we review optoelectronic device applications of topological materials and the inherent topological protection of edge states due to their non-trivial topology. This section is divided into four parts. First, we discuss an important class of topological materials that use valley degree of freedom in applications ranging from quantum computation to optical isolators. Next, we introduce the notion of photonic TIs and their application in optoelectronic devices including TI lasers. Third part deals with the application of TI surface states and topological Dirac states in plasmonic materials and photodetectors. Finally, we discuss about topological flat band and its role in optoelectronics focusing on a recent proposal on Yin-Yang flat bands. In recent years, there have been reviews on optoelectronics using TIs which focused on plasmonics[202-204], photonics[205-207], and valleytronics[208-210]. We provide an overview of each of these subjects. Readers are encouraged to go through individual reviews and references therein for more elaborate details.

4.1 Valleytronics

Valleytronics deals with the design of electronic and optoelectronic devices exploiting the fact that electrons, holes, and excitons behave differently when occupying one valley versus the other. Valleys are local energy minima in the conduction band in association with local maxima in the valence band, where excited carriers are energetically degenerate but differ in crystal momenta. One can also assign a valley pseudospin index denoting the localization of particles in a particular valley[210, 211]. In contrast to spintronics, where electronic spin can be easily manipulated using external fields, it is generally rather difficult to manipulate particles in a valley due to very weak coupling of valley pseudospin to external fields. In addition, the lifetime of particles occupying the valley needs to significantly higher in order to make useful valleytronic devices[208].

Two quantities that can be used to distinguish different valleys to enable, in principle, valleytronic device applications - Berry curvature and orbital magnetic moment. In other words, if two valleys have different Berry curvature and orbital magnetic moment, they can be distinguished by using electric and magnetic fields, respectively. Important material examples are graphene[212], and 2D molybdenum disulfide (MoS_2)[213]; both possess valleys at high-symmetry reciprocal points K and K′ in the Brillouin zone, which are time-reversed images of each other imposed by the underlying hexagonal lattice symmetry.

In the case of MoS_2, inversion symmetry is broken[212] due to staggered structure of its lattice [Fig. 10(a)], which leads to different Berry curvatures at K and K′ and the observation of valley Hall effect in 2014[213]. The two valleys experience opposite effective magnetic field [Fig. 10(b)] allowing for valley polarization under a circularly polarized light, so that electrons from different valleys move in opposite direction under an electrical bias [Fig. 10(c)]. The experimentally measured dependence of anomalous Hall voltage (V_H) on the bias

voltage (V_x) is shown in Fig 10(d). Under R-L modulation V_H scales linearly with V_x, signifying the photoinduced anomalous Hall effect driven by a net valley polarization. Similarly, it can be shown that broken inversion symmetry allows for the existence of orbital magnetic moment responsible for optical circular dichroism and valley optical selection rules[208, 214-216].

In case of MoS_2 inversion symmetry is broken[212] due to staggered structure of its lattice [Fig. 10(a)] which leads to different Berry curvatures at K and K′. Naturally, a valley Hall effect was observed in MoS_2 in 2014[213]. The two valleys experience opposite effective magnetic field [Fig. 10(b)] which allows for valley polarization under a circularly polarized light and the detection of valley Hall effect, i.e., electrons from different valleys move in opposite direction [Fig. 10(c)]. The experimentally measured dependence of anomalous Hall voltage (V_H) on the bias voltage (V_x) is shown in Fig 10(d) for MoS_2 in the presence of circularly polarized light. Under R-L modulation V_H scales linearly with V_x which is a signature of photoinduced anomalous Hall effect driven by a net valley polarization. Similarly, it can also be shown that broken inversion symmetry allows for the existence of orbital magnetic moment responsible for optical circular dichroism and valley optical selection rules[208, 214-216].

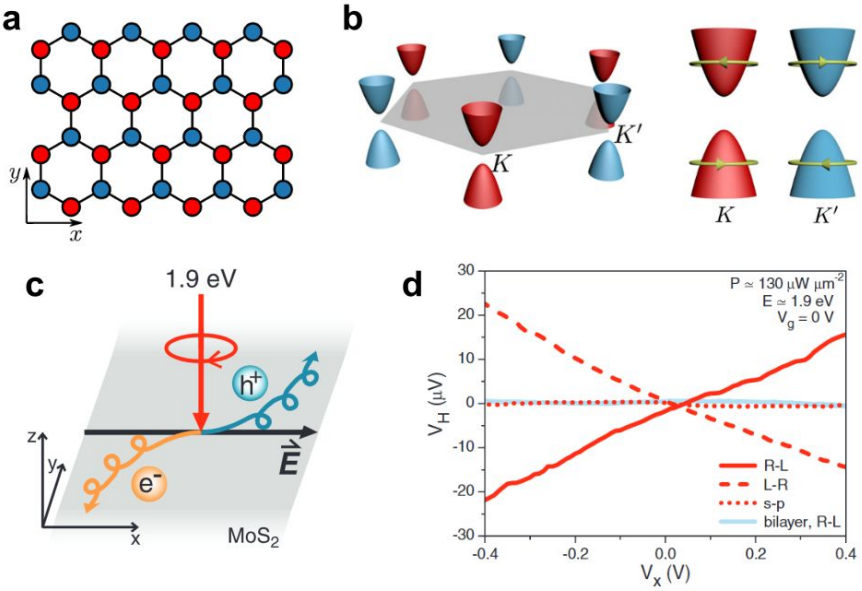

Fig. 10 Valley Hall effect in MoS_2. (a) Schematic of honeycomb lattice with a staggered potential, i.e., sublattices A (red) and B (blue) have different on-site energies, as is the case in MoS_2. (b) Gapped Dirac cones at valley K and K′ with opposite Berry curvature denoted in red and blue respectively. Circularly polarized light of one chirality can excite electrons only in one valley due to opposite effective magnetic field for the two valleys. (c) Upon breaking time reversal symmetry under circularly polarized light, a net valley polarization leads to anomalous Hall effect as carriers in two valleys flow in opposite directions. (d) The source-drain bias (V_x) dependence of Hall voltage (V_H) of monolayer MoS_2 under R-L modulation (red, solid line), under L-R modulation (red, dashed line),

under linear s-p modulation (red, dotted line), and of bilayer MoS_2 under R-L modulation. Linear dependence of V_H on V_x for only R-L and L-R modulation indicates photoinduced valley polarization of monolayer MoS_2 which is absent in bilayer MoS_2. Reprinted with permission from [213], Copyright 2014 Science and from [209], Copyright 2021 Wiley.

The unique valleytronic properties of these 2D materials make them attractive for various applications such as, quantum bit for quantum computation[217-219], quantum key distribution which is an important element of quantum communication relying on generation of polarized photons and remote detection of polarization state[208], and valleytronic-based optical isolators[208] which make use of inherent optical dichroism of valleytronic materials[214-216]. In addition, the topological currents and optoelectronic properties associated with valley effects can be utilized in the design of transistors and efficient switching devices[220-222]. One such application was recently shown[223] using interlayer excitons in van-der-Waals heterostructure of TMDs with a non-volatile memory function, demonstrating a viable route towards valley polarized information processing. Fig. 11(a) shows the schematic of the device consisting of layers of WeS_2 and WS_2 with interlayer excitons (IXs) formed at photon energy of about 1.4 eV [Fig. 11(b)]. Depending on the chemical doping levels the excitons can be in singlet (IX^S at 1.40 eV) [Fig. 11(c)I] or triplet state (IX^T at 1.42 eV) [Fig. 11(c)II] with a lower photoluminescence (PL) intensity of IX^T [Fig. 11(d)]. The valley polarization of excitons can be seen from Fig. 11(e) where the helicity resolved PL data is plotted. IXs show negative circular polarization as evident from a higher cross-polarized (σ^+/σ^-) than the co-polarized (σ^+/σ^+) PL component, which also leads to interesting excitonic hysteresis [Fig. 11(f)] in the degree of valley polarization. These properties of IXs can be used to create valley-addressable memory where the periodic behavior of photon energy of IX emission and PL intensity can be considered analogous to conventional read, write and erase operations while treating the intensity levels of IX^S and IX^T at 1.40 eV and 1.42 eV as bits 0 and 1, respectively, with long retention times as shown in Fig. 11(g).

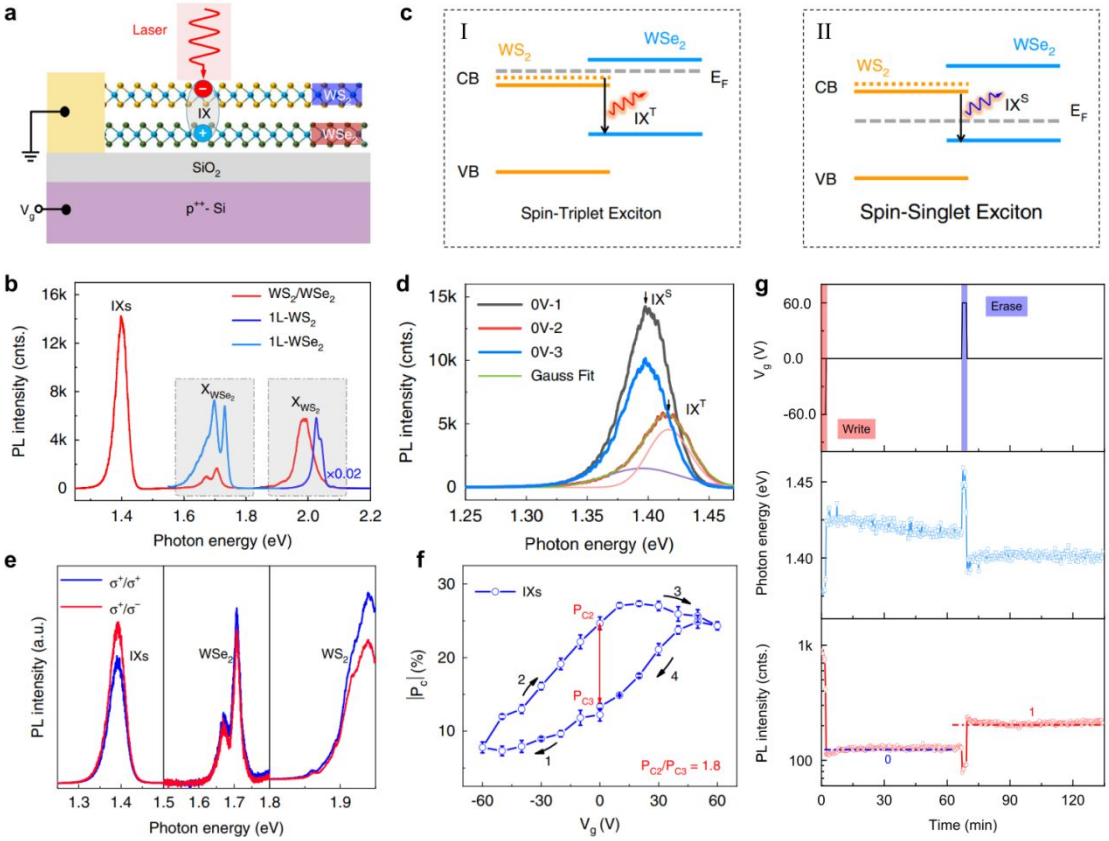

Fig. 11 Memory device using valleytronic properties of TMDs. (a) Schematic of the device containing van-der-Waals heterostructure (HS) of WS_2 and WSe_2 over SiO_2/p^{++}-Si substrate. (b) PL spectra of the HS and monolayer WS_2 and WSe_2. IX represented interlayer exciton. (c) Mechanism for the formation of spin singlet (IX^S) and triplet (IX^T) IX excitons. Dotted yellow line represents upper spin-split conduction band. Gray dashed line denotes the Fermi level. (d) PL spectra of IXs with different scanning sequences (e) Helicity resolved PL spectra with cross-polarized (σ^+/σ^-) and co-polarized (σ^+/σ^+) PL component for inter- and intra-layer excitons. (f) Absolute circular polarization degree, $|P_c| = \left|\frac{I^+ - I^-}{I^+ + I^-}\right|$, where $I^+(I^-)$ indicates co-(cross-) polarized PL component intensity for IX under gate voltage (V_g) sweep. The interlayer hysteresis is caused by change in valley-depolarization times caused by electron/hole doping. (g) Time dependent IX emission characteristics. The PL intensity corresponding to IX^S and IX^T at 1.40 eV and 1.42 eV can be used as bits 0 and 1 respectively. Writing and erasing voltages last for 3 min, while reading lasts for 64 min. Reprinted with permission from [223], Copyright 2022 Springer Nature Limited.

4.2 Topological Photonics

The seminal work by Haldane and Raghu in 2005[224, 225] introduced the notion of topology in electromagnetic waves, leading to the origin of topological photonics. They considered electromagnetic waves in two-dimensional spatially periodic devices embedding time-reversal-breaking magneto-optical elements, so called photonic crystals[226, 227], and illustrated

that the resulting photonic bands would have nontrivial topological invariants. A major source of loss in optical devices that significantly hinders large-scale optical integration in ordinary waveguides is back-scattering[205]. On the other hand, topologically protected waveguides are unidirectional, transmitting electromagnetic waves without back reflection even in the presence of disorder. Topological transport in photonics has unprecedented applications in designing unique devices with immunity to performance degradation due to disorder or outside environment[228-230].

First photonic analogue of quantum Hall effect was realized by Wang et al[231]. A 2D square lattice photonic crystal was prepared using gyromagnetic ferrite rods as shown in Fig. 12(a). The structure was sandwiched between two metallic layers to provide confinement in z-direction. Under the application of magnetic field of magnitude 0.2T, a gap is opened between two topologically non-trivial bands which is depicted in Fig. 12(b) with a gapless forward moving edge state. Numerical simulation [Fig. 12(c)] showed the unidirectionality and immunity to disorder of waveguide at frequency 4.5 GHz which falls within the non-trivial gap. Experimental transmission data confirmed a very low backscattering of this waveguide as shown in Fig. 12(d). Such single mode one-way waveguides have allowed for the novel design of devices for tunable delays and phase shifts with unity transmission[232], reflectionless waveguide bends and splitters[233], signal switches[234], directional filters[235, 236], broadband circulators[237], and slow-light waveguides[238]. A challenge in this direction though has been a weak magnetic response at optical frequencies.

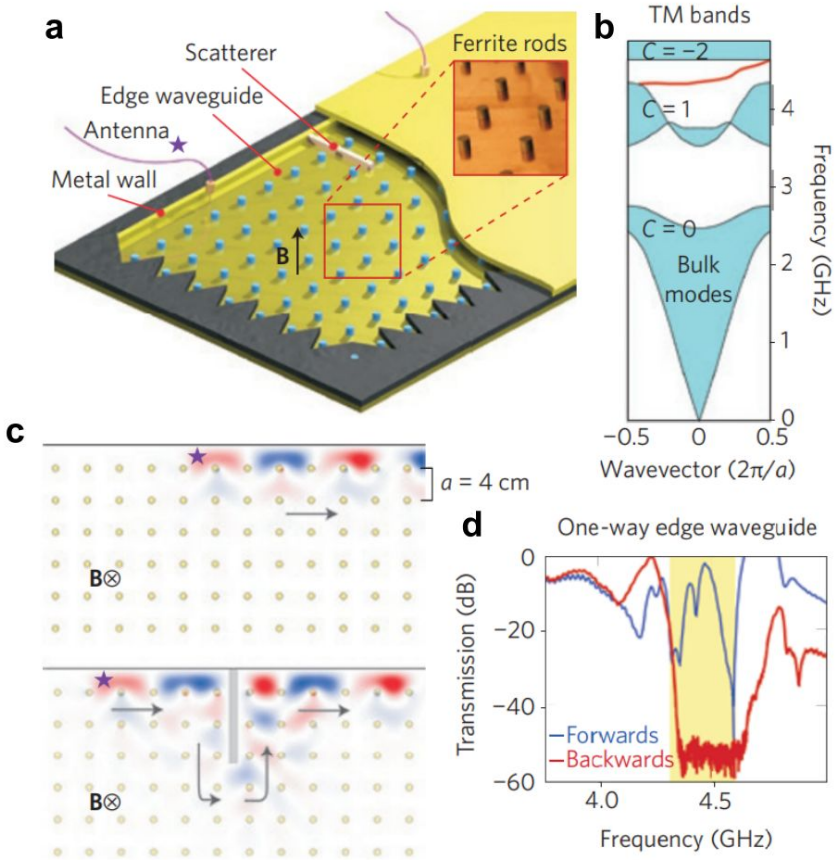

Fig. 12 First experimental demonstration of the topological protection in photonic crystals at microwave frequencies[231]. (a) Gyromagnetic photonic crystal slab with ferrite rods represented by blue dots arranged in a 2D square lattice arrangement. Due to confinement in z-direction by metallic plates this creates 2D transverse magnetic (TM) mode. (b) The TM band structure of one-way gapless edge state between the second and third bands of non-zero Chern numbers. (c) Simulated field propagation of the one-way mode and its topological protection against a long metallic scatterer. (d) The measured robust one-way transmission data of the edge waveguide. The backwards mode is suppressed indicating low backscattering. Reprinted with permission from [205], Copyright 2014 Macmillan Publishers Limited.

Further investigation into the implementation of such models in optical domain led to several ideas to realize photonic topological materials, for example, using polarization of photons as pseudospin in photonic crystals[231, 232, 239], coupled resonators[229, 230, 240], or bianisotropic metamaterials[228]. Subsequently, first photonic TI was introduced in 2013[241] where an array of coupled helical waveguide arranged in a honeycomb lattice led to the topological protection of photon transport realized using periodic modulation inspired by Floquet TIs. Around the same time, an aperiodic coupled ring resonator was also realized experimentally which showed topologically protected photon modes[240]. Since then, there have been many proposals[207, 242-252] both experimental and theoretical to realize a photonic analogue of a solid-state TI.

A vital application of photonic TI is a topological insulator laser which was realized recently[253, 254]. The idea was to use an array of coupled ring resonators phase shifted amongst each other to mimic the effect of imaginary hopping strength in a square lattice [Fig. 13(a)]. The outer perimeter was pumped to promote lasing while inner region had losses. They showed that this topological insulator laser lased in a single mode while a trivial laser showed multi-mode operation [Fig. 13(b)]. The non-trivial laser also had a much higher slope efficiency even in the presence of defects as shown in Fig 13(c). A recent theoretical work showed that indeed the coherence of laser emitters is greatly improved by a topological design[255]. This major break-through has been recognized by many groups to realize more TI lasers[256-258] and move towards a mode-locked pulsed laser[259], a challenge for last few decades. Moreover, recently valleytronic properties have also been realized using topological photonics which finds applications in on-chip communications[260], and quantum cascade lasers[256].

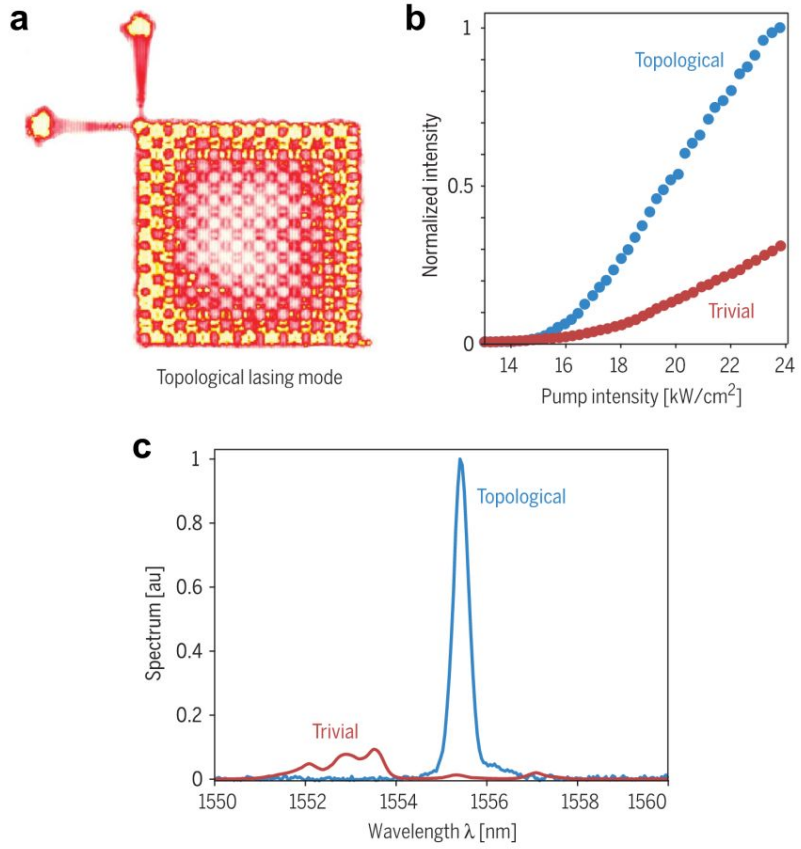

Fig. 13 Topological insulator laser. (a) Top view of lasing pattern in a 10 x 10 cell of topologically connected resonators and output ports. (b) Slope efficiency comparison between trivial and non-trivial lasers. (c) Emission spectrum clearly illustrating the single mode operation of a topological insulator laser. Reprinted with permission from [254], Copyright 2018 Science.

4.3 Plasmonics and Photodetection

Surface plasmon polaritons (referred simply as plasmons) are quanta of elementary excitation that involve collective oscillations of electrons[204, 261, 262]. These charge oscillations are usually confined to the surface of 3D metallic material interfaced with air[204, 261, 262]. In case of TIs, the situation is slightly different due to the presence of a 2D topologically protected surface state sandwiched between two insulators: topological bulk and air.

TI surface states host Dirac plasmon with a plasmon mode dispersion given by[204, 263, 264],

$$\omega_p = \sqrt{\frac{D}{\epsilon_o \epsilon} q} \tag{1}$$

where D is the Drude weight, and ϵ is the effective relative dielectric constant. For TI, $D = \frac{e^2 v_F}{\hbar}\sqrt{\frac{n}{4\pi}}$, very similar to graphene[265] due to a similar relevant charge response and presence of Dirac carriers. Dirac plasmons have been experimentally observed in TIs[266-270] and form one of the major TI device applications for photodetection, especially in the terahertz regime in a field-effect transistor[271-273]. This resonant plasma-wave photodetection in case of TI has been shown to be more efficient than in case of graphene[274]. The utilization and integration of these Dirac plasmons in current Si- based electronic devices was theoretically proposed a few years back[275]. Using first-principles calculations it was shown that a 1/3 monolayer Br coverage on Si-(1,1,1) surface saturates the dangling bonds and forms a uniform $\sqrt{3} \times \sqrt{3}$ $R30°$ honeycomb superstructure [Fig. 14(a)] which generates anisotropic Dirac bands near Fermi level [Fig. 14(b)]. The plasmonic properties of these bands were illustrated by broadened peaks of electron energy loss spectrum (EELS) as shown in Fig. 14(c). The anisotropy of Dirac bands leads to an elliptical dispersion of plasmons which can still be fitted with to the $\sqrt{q}$ relationship in Eqn. (2). Moreover, these Dirac surface states can be protected by using a large-gap 2D material, for example, Boron Nitride, as a protective layer to make such Si-based devices robust[275].

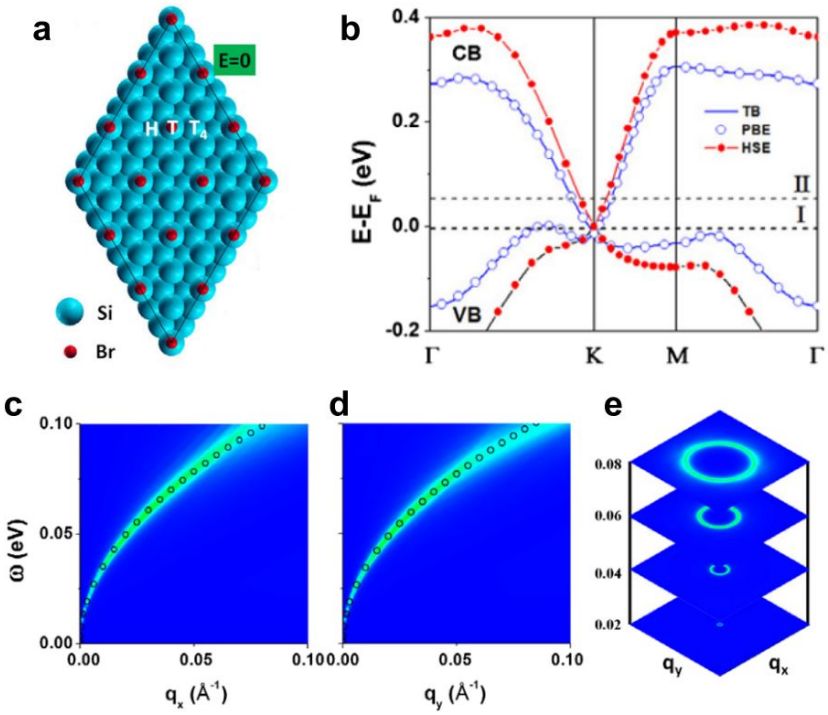

Fig. 14 Si-based terahertz plasmonic device. (a) Schematic of Si-(111) with 1/3 monolayer Br coverage in a $\sqrt{3} \times \sqrt{3} R30°$ supercell. This uniform configuration has the least energy compared with random and cluster configurations. (b) Comparison of band structure obtained using tight-binding (TB) approximation and density functional theory calculation with Perdew-Burke-Ernzerhof (PBE) and Heyd-Scuseria-Ernzerhof (HSE) functionals. (c) and (d) EELS of hole-doped Dirac bands at Fermi energy -0.1 eV in q_x and q_y directions respectively to illustrate the anisotropy due to Dirac bands in the superstructure. The open black circles are fitted to $\omega = \alpha\sqrt{q}$ with $\alpha = 0.35$, and 0.345 $eV/Å^{-1/2}$ for (c) and (d) respectively. (e) 2D momentum space plots of EELS at various excitation energies clearly indicating the elliptical plasmonic dispersion. Reprinted with permission from [275], Copyright 2015 American Physical Society.

A disadvantage of plasmons is their dispersion dependence on carried density (n). Although this dependence allows for gate-voltage tunability, it hinders applications that require a stable excitation frequency in changeable environments[276], leading to unfavorable device operating conditions, for example, low temperature limit, high quality sample requirement, and unstable operation[277]. Recently, a wide range of density dependence of plasmons have been found in topological semi-metals[278, 279], even though they have similar linear electronic dispersion to graphene. Interestingly, there's a possibility of anomalous density independent plasmons (DIP) in 1D carbon nanotubes[280], and nodal surface of electrides[276]. A unified theory of n-independent plasmons was developed recently by Wang et al[277]. DIPs can

fundamentally overcome terahertz-unstable bottlenecks in conventional devices and have been proposed for broadband terahertz spectroscopy in 2D nodal line semi-metallic metamaterials[277].

A unique feature of TI surface state is spin-momentum locking[7, 281]. Zhang et al[282] demonstrated theoretically for a helical metal that a density fluctuation can induce a transverse spin fluctuation and vice versa leading to a spin-plasmon mode. These modes are expected to have a considerably higher lifetime[283] and hence are attractive for device applications[283] like spin-torque oscillators, yet to be observed experimentally[284]. TIs are also known to have non-linear optical properties and enhanced absorbance due to presence of topologically protected gapless surface state[285] and have been reported to exhibit broad spectrum photodetection[286-290]. Recently, with a growing interest[291-293] in flexible optoelectronics given their potential applications in wearable devices, sensors, and communication[291-295], a TI based flexible photodetector has been fabricated by depositing thin films of Bi_2Te_3, a well-known TI[17] onto a flexible plastic substrate, PET (Polyethylene terephthalate)[296]. Fig 15(a) shows the schematic of photodetector device and the flexibility of deposited film. The photocurrent response for near infrared regime is shown in Fig 15(b). As can be seen clearly the device detects the on and off laser mode. This high photo-response is speculated to be due to the band transitions and electron-pair generation between valence bulk band and conduction surface band as depicted in Fig. 15(c), but no certain theoretical or experimental evidence has been reported yet.

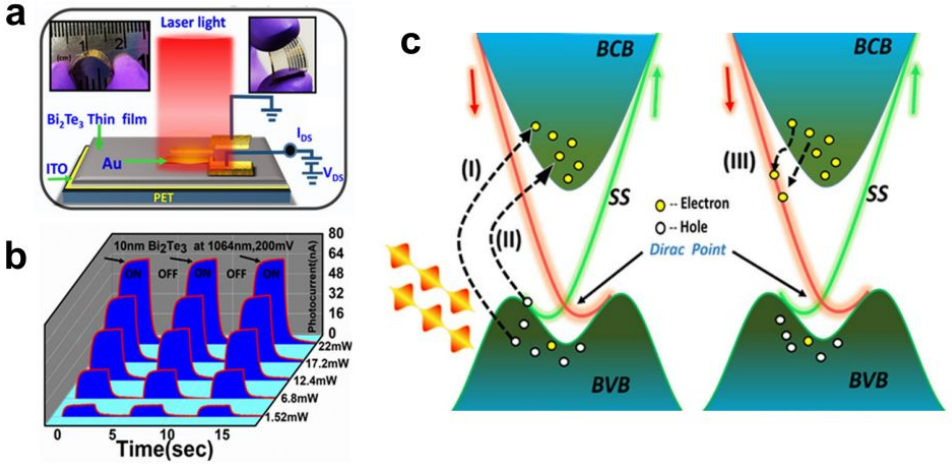

Fig. 15 TI based flexible photodetector. (a) Schematic of photodetector device. Inset shows the flexibility of TI thin film. (b) Power dependent photocurrent response of flexible TI. (c) Depiction of a possible mechanism for the high performance of flexible TI. BV/CB – Bulk Valence/Conduction Band; SS – Surface State Reprinted with permission from [296], Copyright 2021 Scientific Reports.

4.4 Topological flat bands

Analogous to Haldane's proposal for Integer Quantum Hall Effect (IQHE), Fractional Chern Insulators (FCIs) have been proposed and numerically shown to be stabilized in topological flat bands (FBs)[39, 297-301]. These FBs are counterpart of Landau Levels (LLs) of 2D free electron gas, with Chern number equal to 1, and arise due to the destructive interference of Bloch waves in a lattice system. This interference manifests itself into compact localized states in real space giving FBs macroscopic degeneracy, similar to LLs[11, 37]. The infinite effective mass of carriers and hence their quenched kinetic energy in FBs allow the interactions to dominate leading to the stabilization of a variety of interaction-mediated exotic phases, such as Wigner crystallization[45, 302], high temperature superconductivity[47, 303], ferromagnetism[304-309], Mottness[24, 25], Fractional QHE[38, 310-312], excitonic BEC[53] and TIs[313-320].

A most widely used FB electronic lattice is a 2D Kagome lattice[310, 321-324]. Depending on the sign of hopping integral within nearest-neighbor TB framework, this lattice hosts a FB either on the top or the bottom of the energy spectrum[310, 322]. Recently, as an extension of Kagome lattice, a novel 2D lattice was introduced, called diatomic Kagome lattice[325-327] [Fig 16(a)] containing two sets of Kagome bands. There is a rich phase diagram of band structures possible for this lattice in the parameter space of hopping integrals[326]. An intriguing band structure arises for certain hopping parameters which gives rise to enantiomorphic, i.e., Yin-Yang FBs[326, 327]. Under this configuration of bands, the FBs of the two sets of Kagome bands face each other forming the valence and conduction bands, both topologically non-trivial and flat but with opposite Chern numbers due to opposite effective signs of hopping integrals for the two sets. This fascinating band structure, called the Yin-Yang bands [Fig 16(b)], constituting a new class of "quantum semiconductors". It has been shown to exist in material systems, like anilato-based metal-organic frameworks[325], superatomic graphene[50, 327] and bilayer nickel-bis(dithiolene)[327] based on density functional theory calculations, while the superatomic graphene has been recently already made experimentally[54]. Interestingly, this unique band structure is speculated to show unconventional and exotic physics like, giant circular dichroism (CD)[326], anomalous excitonic behavior[50, 53], and topological superconductivity[328].

Unconventional optical properties of Yin-Yang bands provide a perfect platform for topological FB optoelectronic device applications. The stabilization of a triplet excitonic insulator state[50] suggest the possibility of a complete population inversion between these bands, a property crucial for the realization of a solid-state laser. In addition, due to a flat conduction and valence band the coherence in wavefunction is naturally present which makes it an ideal candidate for a single mode cavity-free ultralow threshold laser. Two proposals for FB devices based on Yin-Yang bands were given by Yinong et al[326] and are elaborated here in Fig. 16(c). Interestingly, Yin-Yang FBs allow for the possibility of quantization of photoexcited FB Hall conductivity[327]. One can take advantage of this quantization to build

robust topological photodetectors in a photovoltaic cell, as illustrated in Figs. 16(c)I and 16(c)II. Also, the flat Chern bands in whole Brillouin zone contribute to the CD effect in one chirality without the need to select one of the two sets of valleys, as in valleytronics[210], whose CD effects would cancel out each other. This will enable to build CP lasers in a heterojunction diode, as illustrated in Figs. 16(c)III and 16(c)IV.

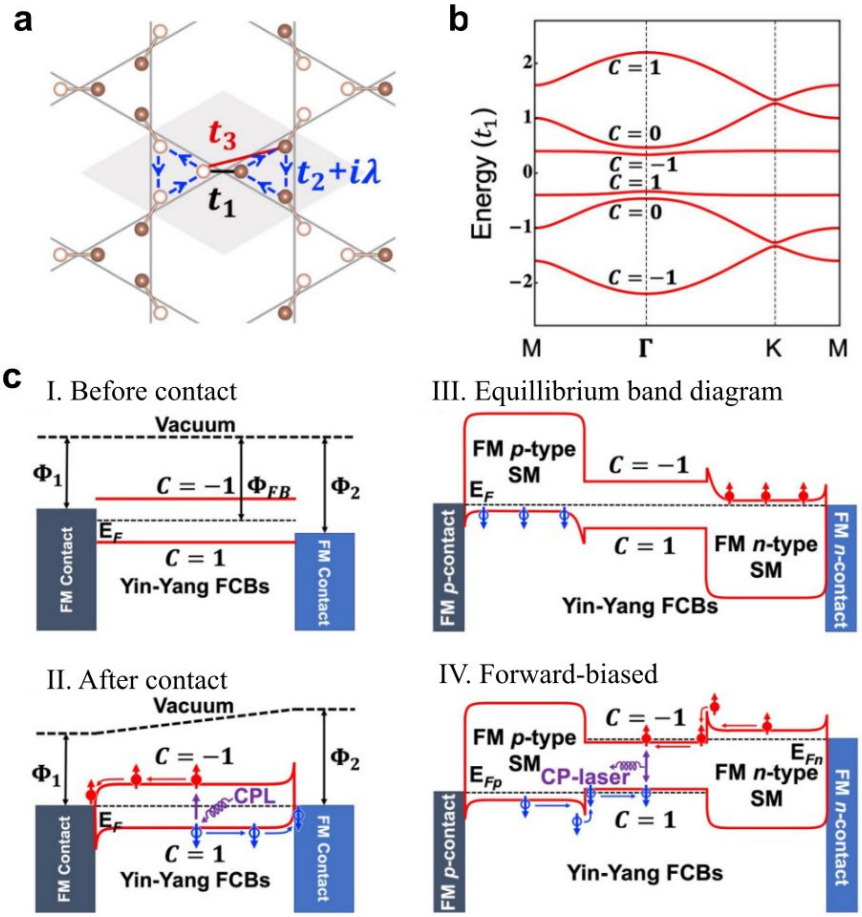

Fig. 16 (a) The diatomic Kagome lattice structure, where t_1, t_2, and t_3 are hopping integrals and λ represents the SOC strength. (b) The ideal yin-yang Kagome band structure and Chern numbers of each band with SOC. (c) Schematic band diagrams of two flat bands device setups. (a) The band diagrams of the yin-yang FCBs and two ferromagnetic (FM) metal contacts with different work functions $\Phi_{1,2}$ before contact in a photovoltaic cell. The Chern numbers are opposite for yin and yang FCBs. (b) The band diagram after contact. A σ + CPL excitation creates a spin-up electron in the top yang FCB and leave behind a spin-down hole in the bottom yin FCB. The electron (hole) flows to the left (right) FM contact with a smaller (larger) work function. (c) The equilibrium band diagram of a spin-polarized double heterostructure made of a FM p contact/FM p-type semiconductor (SM)/yin-yang FCB material/FM n-type SM/FM n contact. The Fermi level EF is constant across the junction. (d) The band diagram after a forward bias applied to (c) where the spin-up electrons and spin-down holes are injected into yang and yin FCBs, respectively, and the electron-hole recombination emits a

CP laser. E_{F_n} (E_{F_p}) represents the quasi-Fermi level of electrons (holes). Reprinted with permission from [326], Copyright 2020 American Physical Society.

5. Summary and outlook

In this review, we have presented a concise updated review on device technologies utilizing unique spin, electronic and optical properties of topological materials. The guiding principle behind this review has been to illustrate the unique physical properties of topological materials and define their critical role in the development of new spintronic, electronic, and optical quantum device technologies. In topological spintronic devices, several novel approaches to achieve high spin-polarization current have been elaborated in various systems e.g., curved 2D TIs through strain engineering, heterostructures based on TI and FM, traditional semiconductors and 2D transition metal dichalcogenides with topological 1D dislocations, and 2D materials with non-centrosymmetric symmetry. In topological electronic devices, the aspiring exploration of different topological materials based on distinct physical mechanisms in field effect transistors has been retrospected, followed by a concise review of topological p-n junctions and recent proposals of other topological electronic devices. In topological optoelectronic devices, recent progress of the topological photodetector and topological laser have been briefly review based on the formation of topological plasmon polaritons and photonic TIs, respectively. At last, an intriguing and exciting novel topological yin-yang flat-bands system is illustrated in detail for its promising applications in topological optoelectronics.

With the fast development of topological materials, their applications in various fields have been broadly explored. The progresses in all these fields are inspiring, and one of the most promising applications of topological materials has been well recognized in the field of magnetic devices, i.e., topological spintronics, due to their outstanding spin-to-charge and charge-to-spin interconversion that arises from their topological nature. We can anticipate the emergence of a series novel magnetic device based on topological materials in the near future. On the other hand, the studies of topological electronic and optoelectronic devices are awaiting some essential breakthroughs, especially in the experimental perspective, to compete with the current mature technology based on traditional electronic and optoelectronic materials. Yet, they may supplement the current technologies in some special targeted applications. The study of topological materials has spawned a much more collaborative community that has united researchers from various fields, which will surely facilitate exploration of topological materials in technologies beyond what have been covered here. New applications based on novel topological materials will remain one of the most attractive research fields in the near future.

Conflicts of Interest

The authors do not have conflict of interests to declare.

Acknowledgements

K.-H.J. acknowledges the support from the Institute for Basic Science (Grant No. IBS-R014-Y1). W. J. acknowledges the support from National Natural Science Foundation of China (Grant No. NSFC-12204037) and Beijing Institute of Technology Research Fund Program for Young Scholars. G.S. and F.L. are supported by U.S. DOE-BES (Grant No. DE-FG02-04ER46148).

References

1. Thouless, D. J.; Kohmoto, M.; Nightingale, M. P.; den Nijs, M. Quantized Hall Conductance in a Two-Dimensional Periodic Potential. *Phys. Rev. Lett.* **1982,** 49, (6), 405-408.
2. Klitzing, K. v.; Dorda, G.; Pepper, M. New Method for High-Accuracy Determination of the Fine-Structure Constant Based on Quantized Hall Resistance. *Phys. Rev. Lett.* **1980,** 45, (6), 494-497.
3. Haldane, F. D. M. Model for a Quantum Hall Effect without Landau Levels: Condensed-Matter Realization of the "Parity Anomaly". *Phys. Rev. Lett.* **1988,** 61, (18), 2015-2018.
4. Kane, C. L.; Mele, E. J. Z_2 Topological Order and the Quantum Spin Hall Effect. *Phys. Rev. Lett.* **2005,** 95, (14), 146802.
5. Kane, C. L.; Mele, E. J. Quantum Spin Hall Effect in Graphene. *Phys. Rev. Lett.* **2005,** 95, (22), 226801.
6. Bernevig, B. A.; Hughes, T. L.; Zhang, S.-C. Quantum Spin Hall Effect and Topological Phase Transition in HgTe Quantum Wells. *Science* **2006,** 314, (5806), 1757-1761.
7. Hasan, M. Z.; Kane, C. L. Colloquium: Topological insulators. *Rev. Mod. Phys.* **2010,** 82, (4), 3045-3067.
8. Ando, Y.; Fu, L. Topological Crystalline Insulators and Topological Superconductors: From Concepts to Materials. *Annu. Rev. Condens. Matter. Phys.* **2015,** 6, (1), 361-381.
9. Armitage, N. P.; Mele, E. J.; Vishwanath, A. Weyl and Dirac semimetals in three-dimensional solids. *Rev. Mod. Phys.* **2018,** 90, (1), 015001.
10. Sato, M.; Ando, Y. Topological superconductors: a review. *Rep. Prog. Phys.* **2017,** 80, (7), 076501.
11. Liu, Z.; Liu, F.; Wu, Y.-S. Exotic electronic states in the world of flat bands: From theory to material. *Chin. Phys. B* **2014,** 23, (7), 77308-77308.
12. Maciejko, J.; Hughes, T. L.; Zhang, S.-C. The Quantum Spin Hall Effect. *Annu. Rev. Condens. Matter. Phys.* **2011,** 2, (1), 31-53.
13. Wang, Z. F.; Jin, K.-H.; Liu, F. Computational design of two-dimensional topological materials. *WIREs Comput. Mol. Sci.* **2017,** 7, (4), e1304.
14. Wang, Z. F.; Jin, K.-H.; Liu, F. Quantum spin Hall phase in 2D trigonal lattice. *Nat. Commun.* **2016,** 7, (1), 12746.
15. Jiang, W.; Ni, X.; Liu, F. Exotic Topological Bands and Quantum States in Metal–Organic and Covalent–Organic Frameworks. *Acc. Chem. Res.* **2021,** 54, (2), 416-426.

16. Zhang, H.; Liu, C.-X.; Qi, X.-L.; Dai, X.; Fang, Z.; Zhang, S.-C. Topological insulators in Bi_2Se_3, Bi_2Te_3 and Sb_2Te_3 with a single Dirac cone on the surface. *Nat. Phys.* **2009,** 5, (6), 438-442.
17. Chen, Y. L.; Analytis, J. G.; Chu, J. H.; Liu, Z. K.; Mo, S. K.; Qi, X. L.; Zhang, H. J.; Lu, D. H.; Dai, X.; Fang, Z.; Zhang, S. C.; Fisher, I. R.; Hussain, Z.; Shen, Z. X. Experimental Realization of a Three-Dimensional Topological Insulator, Bi_2Te_3. *Science* **2009,** 325, (5937), 178-181.
18. Fu, L. Topological Crystalline Insulators. *Phys. Rev. Lett.* **2011,** 106, (10), 106802.
19. Hsieh, T. H.; Lin, H.; Liu, J.; Duan, W.; Bansil, A.; Fu, L. Topological crystalline insulators in the SnTe material class. *Nat. Commun.* **2012,** 3, (1), 982.
20. Schindler, F.; Wang, Z.; Vergniory, M. G.; Cook, A. M.; Murani, A.; Sengupta, S.; Kasumov, A. Y.; Deblock, R.; Jeon, S.; Drozdov, I.; Bouchiat, H.; Guéron, S.; Yazdani, A.; Bernevig, B. A.; Neupert, T. Higher-order topology in bismuth. *Nat. Phys.* **2018,** 14, (9), 918-924.
21. Schindler, F.; Cook, A. M.; Vergniory, M. G.; Wang, Z.; Parkin, S. S. P.; Bernevig, B. A.; Neupert, T. Higher-order topological insulators. *Sci. Adv.* **2018,** 4, (6), eaat0346.
22. Trifunovic, L.; Brouwer, P. W. Higher-Order Bulk-Boundary Correspondence for Topological Crystalline Phases. *Phys. Rev. X* **2019,** 9, (1), 011012.
23. Lu, F.; Zhao, J.; Weng, H.; Fang, Z.; Dai, X. Correlated Topological Insulators with Mixed Valence. *Phys. Rev. Lett.* **2013,** 110, (9), 096401.
24. Lee, J.; Jin, K.-H.; Catuneanu, A.; Go, A.; Jung, J.; Won, C.; Cheong, S.-W.; Kim, J.; Liu, F.; Kee, H.-Y.; Yeom, H. W. Honeycomb-Lattice Mott Insulator on Tantalum Disulphide. *Phys. Rev. Lett.* **2020,** 125, (9), 096403.
25. Lee, D.; Jin, K.-H.; Liu, F.; Yeom, H. W. Tunable Mott Dirac and Kagome Bands Engineered on 1T-TaS_2. *Nano Lett.* **2022,** 22, (19), 7902-7909.
26. Wang, Z. F.; Zhang, H.; Liu, D.; Liu, C.; Tang, C.; Song, C.; Zhong, Y.; Peng, J.; Li, F.; Nie, C.; Wang, L.; Zhou, X. J.; Ma, X.; Xue, Q. K.; Liu, F. Topological edge states in a high-temperature superconductor FeSe/$SrTiO_3$(001) film. *Nat. Mater.* **2016,** 15, (9), 968-973.
27. Jin, K.-H.; Huang, H.; Mei, J.-W.; Liu, Z.; Lim, L.-K.; Liu, F. Topological superconducting phase in high-Tc superconductor MgB_2 with Dirac–nodal-line fermions. *npj Comput. Mater.* **2019,** 5, (1), 57.
28. Zhou, X.; Gordon, K. N.; Jin, K.-H.; Li, H.; Narayan, D.; Zhao, H.; Zheng, H.; Huang, H.; Cao, G.; Zhigadlo, N. D.; Liu, F.; Dessau, D. S. Observation of topological surface states in the high-temperature superconductor MgB_2. *Phys. Rev. B* **2019,** 100, (18), 184511.
29. Zhang, X.; Jin, K.-H.; Mao, J.; Zhao, M.; Liu, Z.; Liu, F. Prediction of intrinsic topological superconductivity in Mn-doped GeTe monolayer from first-principles. *npj Comput. Mater.* **2021,** 7, (1), 44.
30. Chen, J.; He, J.; Pan, D.; Wang, X.; Yang, N.; Zhu, J.; Yang, S. A.; Zhang, G. Emerging theory and phenomena in thermal conduction: A selective review. *Sci. China Phys. Mech. Astron.* **2022,** 65, (11), 117002.
31. Wang, X.; Yang, T.; Cheng, Z.; Surucu, G.; Wang, J.; Zhou, F.; Zhang, Z.; Zhang, G. Topological nodal line phonons: Recent advances in materials realization. *Appl. Phys. Rev.* **2022,** 9, (4).
32. McClarty, P. A. Topological Magnons: A Review. *Annu. Rev. Condens. Matter Phys.* **2022,** 13, (1), 171-190.
33. In, C.; Choi, H. Dirac Fermion and Plasmon Dynamics in Graphene and 3D Topological

Insulators. *Adv. Optical Mater.* **2020,** 8, (3), 1801334.
34. Bergman, D. L.; Wu, C.; Balents, L. Band touching from real-space topology in frustrated hopping models. *Phys. Rev. B* **2008,** 78, (12), 125104.
35. Rhim, J.-W.; Yang, B.-J. Classification of flat bands according to the band-crossing singularity of Bloch wave functions. *Phys. Rev. B* **2019,** 99, (4), 045107.
36. Rhim, J.-W.; Kim, K.; Yang, B.-J. Quantum distance and anomalous Landau levels of flat bands. *Nature* **2020,** 584, (7819), 59-63.
37. Liu, H.; Sethi, G.; Meng, S.; Liu, F. Orbital design of flat bands in non-line-graph lattices via line-graph wave functions. *Phys. Rev. B* **2022,** 105, (8), 085128.
38. Neupert, T.; Santos, L.; Chamon, C.; Mudry, C. Fractional Quantum Hall States at Zero Magnetic Field. *Phys. Rev. Lett.* **2011,** 106, (23), 236804-236804.
39. Sheng, D. N.; Gu, Z.-C.; Sun, K.; Sheng, L. Fractional quantum Hall effect in the absence of Landau levels. *Nat. Commun.* **2011,** 2, (1), 389-389.
40. Parameswaran, S. A.; Roy, R.; Sondhi, S. L. Fractional quantum Hall physics in topological flat bands. *C. R. Phys.* **2013,** 14, (9), 816-839.
41. Mielke, A.; Tasaki, H. Ferromagnetism in the Hubbard model. *Commun. Math. Phys.* **1993,** 158, (2), 341-371.
42. Tasaki, H. From Nagaoka's Ferromagnetism to Flat-Band Ferromagnetism and Beyond: An Introduction to Ferromagnetism in the Hubbard Model. *Prog. Theor. Phys.* **1998,** 99, (4), 489-548.
43. Hase, I.; Yanagisawa, T.; Aiura, Y.; Kawashima, K. Possibility of Flat-Band Ferromagnetism in Hole-Doped Pyrochlore Oxides $Sn_2Nb_2O_7$ and $Sn_2Ta_2O_7$. *Phys. Rev. Lett.* **2018,** 120, (19), 196401.
44. Zhou, Y.; Jin, K.-H.; Huang, H.; Wang, Z.; Liu, F. Weyl points created by a three-dimensional flat band. *Phys. Rev. B* **2019,** 99, (20), 201105.
45. Wu, C.; Bergman, D.; Balents, L.; Das Sarma, S. Flat Bands and Wigner Crystallization in the Honeycomb Optical Lattice. *Phys. Rev. Lett.* **2007,** 99, (7), 70401-70401.
46. Jaworowski, B.; Güçlü, A. D.; Kaczmarkiewicz, P.; Kupczyński, M.; Potasz, P.; Wójs, A. Wigner crystallization in topological flat bands. *New J. Phys.* **2018,** 20, (6), 063023.
47. Miyahara, S.; Kusuta, S.; Furukawa, N. BCS theory on a flat band lattice. *Physica C: Superconductivity* **2007,** 460-462, 1145-1146.
48. Volovik, G. E. Graphite, Graphene, and the Flat Band Superconductivity. *JETP Lett.* **2018,** 107, (8), 516-517.
49. Aoki, H. Theoretical Possibilities for Flat Band Superconductivity. *J. Supercond. Nov. Magn.* **2020,** 33, (8), 2341-2346.
50. Sethi, G.; Zhou, Y.; Zhu, L.; Yang, L.; Liu, F. Flat-Band-Enabled Triplet Excitonic Insulator in a Diatomic Kagome Lattice. *Phys. Rev. Lett.* **2021,** 126, (19), 196403-196403.
51. Julku, A.; Bruun, G. M.; Törmä, P. Quantum Geometry and Flat Band Bose-Einstein Condensation. *Phys. Rev. Lett.* **2021,** 127, (17), 170404.
52. Julku, A.; Bruun, G. M.; Törmä, P. Excitations of a Bose-Einstein condensate and the quantum geometry of a flat band. *Phys. Rev. B* **2021,** 104, (14), 144507.
53. Sethi, G.; Cuma, M.; Liu, F. Excitonic Condensate in Flat Valence and Conduction Bands of Opposite Chirality. *Phys. Rev. Lett.* **2023,** 130, (18), 186401
54. Delgado, A.; Dusold, C.; Jiang, J.; Cronin, A.; Louie, S. G.; Fischer, F. R. Evidence for excitonic insulator ground state in triangulene Kagome lattice. *arXiv:2301.06171* **2023**.

55. König, M.; Wiedmann, S.; Brüne, C.; Roth, A.; Buhmann, H.; Molenkamp, L. W.; Qi, X.-L.; Zhang, S.-C. Quantum Spin Hall Insulator State in HgTe Quantum Wells. *Science* **2007,** 318, (5851), 766-770.
56. Li, C. H.; van 't Erve, O. M. J.; Robinson, J. T.; Liu, Y.; Li, L.; Jonker, B. T. Electrical detection of charge-current-induced spin polarization due to spin-momentum locking in Bi2Se3. *Nat. Nanotech.* **2014,** 9, (3), 218-224.
57. Mellnik, A. R.; Lee, J. S.; Richardella, A.; Grab, J. L.; Mintun, P. J.; Fischer, M. H.; Vaezi, A.; Manchon, A.; Kim, E. A.; Samarth, N.; Ralph, D. C. Spin-transfer torque generated by a topological insulator. *Nature* **2014,** 511, (7510), 449-451.
58. Frolov, S. M.; Manfra, M. J.; Sau, J. D. Topological superconductivity in hybrid devices. *Nat. Phys.* **2020,** 16, (7), 718-724.
59. Bernevig, B. A.; Zhang, S.-C. Quantum Spin Hall Effect. *Phys. Rev. Lett.* **2006,** 96, (10), 106802.
60. Jin, K.-H.; Jhi, S.-H. Spin rectification by orbital polarization in Bi-bilayer nanoribbons. *Phys. Chem. Chem. Phys.* **2016,** 18, (12), 8637-8642.
61. Huang, B.; Jin, K.-H.; Cui, B.; Zhai, F.; Mei, J.; Liu, F. Bending strain engineering in quantum spin hall system for controlling spin currents. *Nat. Commun.* **2017,** 8, (1), 15850.
62. Zhang, L. Z.; Zhai, F.; Jin, K.-H.; Cui, B.; Huang, B.; Wang, Z.; Lu, J. Q.; Liu, F. Quantum Spin Hall Effect and Tunable Spin Transport in As-Graphane. *Nano Lett.* **2017,** 17, (7), 4359-4364.
63. Jin, K.-H.; Jhi, S.-H.; Liu, F. Nanostructured topological state in bismuth nanotube arrays: inverting bonding–antibonding levels of molecular orbitals. *Nanoscale* **2017,** 9, (43), 16638-16644.
64. Morpurgo, A. F.; Guinea, F. Intervalley Scattering, Long-Range Disorder, and Effective Time-Reversal Symmetry Breaking in Graphene. *Phys. Rev. Lett.* **2006,** 97, (19), 196804.
65. Levy, N.; Burke, S. A.; Meaker, K. L.; Panlasigui, M.; Zettl, A.; Guinea, F.; Neto, A. H. C.; Crommie, M. F. Strain-Induced Pseudo-Magnetic Fields Greater Than 300 Tesla in Graphene Nanobubbles. *Science* **2010,** 329, (5991), 544-547.
66. Li, Z.; Lv, Y.; Ren, L.; Li, J.; Kong, L.; Zeng, Y.; Tao, Q.; Wu, R.; Ma, H.; Zhao, B.; Wang, D.; Dang, W.; Chen, K.; Liao, L.; Duan, X.; Duan, X.; Liu, Y. Efficient strain modulation of 2D materials via polymer encapsulation. *Nat. Commun.* **2020,** 11, (1), 1151.
67. McGilly, L. J.; Kerelsky, A.; Finney, N. R.; Shapovalov, K.; Shih, E.-M.; Ghiotto, A.; Zeng, Y.; Moore, S. L.; Wu, W.; Bai, Y.; Watanabe, K.; Taniguchi, T.; Stengel, M.; Zhou, L.; Hone, J.; Zhu, X.; Basov, D. N.; Dean, C.; Dreyer, C. E.; Pasupathy, A. N. Visualization of moiré superlattices. *Nat. Nanotechnol.* **2020,** 15, (7), 580-584.
68. Büttiker, M. Absence of backscattering in the quantum Hall effect in multiprobe conductors. *Phys. Rev. B* **1988,** 38, (14), 9375-9389.
69. Prinz, V. Y.; Seleznev, V. A.; Gutakovsky, A. K.; Chehovskiy, A. V.; Preobrazhenskii, V. V.; Putyato, M. A.; Gavrilova, T. A. Free-standing and overgrown InGaAs/GaAs nanotubes, nanohelices and their arrays. *Physica E* **2000,** 6, (1), 828-831.
70. Schmidt, O. G.; Eberl, K. Thin solid films roll up into nanotubes. *Nature* **2001,** 410, (6825), 168-168.
71. Huang, M.; Boone, C.; Roberts, M.; Savage, D. E.; Lagally, M. G.; Shaji, N.; Qin, H.; Blick, R.; Nairn, J. A.; Liu, F. Nanomechanical Architecture of Strained Bilayer Thin Films: From Design Principles to Experimental Fabrication. *Adv. Mater.* **2005,** 17, (23), 2860-2864.

72. Murakami, S. Quantum Spin Hall Effect and Enhanced Magnetic Response by Spin-Orbit Coupling. *Phys. Rev. Lett.* **2006,** 97, (23), 236805.
73. Yang, F.; Miao, L.; Wang, Z. F.; Yao, M.-Y.; Zhu, F.; Song, Y. R.; Wang, M.-X.; Xu, J.-P.; Fedorov, A. V.; Sun, Z.; Zhang, G. B.; Liu, C.; Liu, F.; Qian, D.; Gao, C. L.; Jia, J.-F. Spatial and Energy Distribution of Topological Edge States in Single Bi(111) Bilayer. *Phys. Rev. Lett.* **2012,** 109, (1), 016801.
74. Kim, S. H.; Jin, K.-H.; Park, J.; Kim, J. S.; Jhi, S.-H.; Kim, T.-H.; Yeom, H. W. Edge and interfacial states in a two-dimensional topological insulator: Bi(111) bilayer on Bi_2Te_2Se. *Phys. Rev. B* **2014,** 89, (15), 155436.
75. Drozdov, I. K.; Alexandradinata, A.; Jeon, S.; Nadj-Perge, S.; Ji, H.; Cava, R. J.; Andrei Bernevig, B.; Yazdani, A. One-dimensional topological edge states of bismuth bilayers. *Nat. Phys.* **2014,** 10, (9), 664-669.
76. Jin, K.-H.; Jhi, S.-H. Quantum anomalous Hall and quantum spin-Hall phases in flattened Bi and Sb bilayers. *Sci. Rep.* **2015,** 5, (1), 8426.
77. Sabater, C.; Gosálbez-Martínez, D.; Fernández-Rossier, J.; Rodrigo, J. G.; Untiedt, C.; Palacios, J. J. Topologically Protected Quantum Transport in Locally Exfoliated Bismuth at Room Temperature. *Phys. Rev. Lett.* **2013,** 110, (17), 176802.
78. Zang, J.; Huang, M.; Liu, F. Mechanism for Nanotube Formation from Self-Bending Nanofilms Driven by Atomic-Scale Surface-Stress Imbalance. *Phys. Rev. Lett.* **2007,** 98, (14), 146102.
79. Zhou, M.; Ming, W.; Liu, Z.; Wang, Z.; Yao, Y.; Liu, F. Formation of quantum spin Hall state on Si surface and energy gap scaling with strength of spin orbit coupling. *Sci. Rep.* **2014,** 4, (1), 7102.
80. Zhou, M.; Ming, W.; Liu, Z.; Wang, Z.; Li, P.; Liu, F. Epitaxial growth of large-gap quantum spin Hall insulator on semiconductor surface. *Proc. Natl Acad. Sci.* **2014,** 111, (40), 14378-14381.
81. Reis, F.; Li, G.; Dudy, L.; Bauernfeind, M.; Glass, S.; Hanke, W.; Thomale, R.; Schäfer, J.; Claessen, R. Bismuthene on a SiC substrate: A candidate for a high-temperature quantum spin Hall material. *Science* **2017,** 357, (6348), 287-290.
82. Li, C.; Jin, K.-H.; Zhang, S.; Wang, F.; Jia, Y.; Liu, F. Formation of a large gap quantum spin Hall phase in a 2D trigonal lattice with three p-orbitals. *Nanoscale* **2018,** 10, (12), 5496-5502.
83. Chun, I. S.; Li, X. Controlled Assembly and Dispersion of Strain-Induced InGaAs/GaAs Nanotubes. *IEEE Trans. Nanotechnol.* **2008,** 7, (4), 493-495.
84. Wolf, S. A.; Awschalom, D. D.; Buhrman, R. A.; Daughton, J. M.; Molnár, S. v.; Roukes, M. L.; Chtchelkanova, A. Y.; Treger, D. M. Spintronics: A Spin-Based Electronics Vision for the Future. *Science* **2001,** 294, (5546), 1488-1495.
85. Žutić, I.; Fabian, J.; Das Sarma, S. Spintronics: Fundamentals and applications. *Rev. Mod. Phys.* **2004,** 76, (2), 323-410.
86. Burkov, A. A.; Hawthorn, D. G. Spin and Charge Transport on the Surface of a Topological Insulator. *Phys. Rev. Lett.* **2010,** 105, (6), 066802.
87. Tserkovnyak, Y.; Loss, D. Thin-Film Magnetization Dynamics on the Surface of a Topological Insulator. *Phys. Rev. Lett.* **2012,** 108, (18), 187201.
88. Fan, Y.; Upadhyaya, P.; Kou, X.; Lang, M.; Takei, S.; Wang, Z.; Tang, J.; He, L.; Chang, L.-T.; Montazeri, M.; Yu, G.; Jiang, W.; Nie, T.; Schwartz, R. N.; Tserkovnyak, Y.; Wang, K. L. Magnetization switching through giant spin–orbit torque in a magnetically doped topological

insulator heterostructure. *Nat. Mater.* **2014,** 13, (7), 699-704.
89. Katmis, F.; Lauter, V.; Nogueira, F. S.; Assaf, B. A.; Jamer, M. E.; Wei, P.; Satpati, B.; Freeland, J. W.; Eremin, I.; Heiman, D.; Jarillo-Herrero, P.; Moodera, J. S. A high-temperature ferromagnetic topological insulating phase by proximity coupling. *Nature* **2016,** 533, (7604), 513-516.
90. Chen, Y. L.; Chu, J.-H.; Analytis, J. G.; Liu, Z. K.; Igarashi, K.; Kuo, H.-H.; Qi, X. L.; Mo, S. K.; Moore, R. G.; Lu, D. H.; Hashimoto, M.; Sasagawa, T.; Zhang, S. C.; Fisher, I. R.; Hussain, Z.; Shen, Z. X. Massive Dirac Fermion on the Surface of a Magnetically Doped Topological Insulator. *Science* **2010,** 329, (5992), 659-662.
91. Wray, L. A.; Xu, S.-Y.; Xia, Y.; Hsieh, D.; Fedorov, A. V.; Hor, Y. S.; Cava, R. J.; Bansil, A.; Lin, H.; Hasan, M. Z. A topological insulator surface under strong Coulomb, magnetic and disorder perturbations. *Nat. Phys.* **2011,** 7, (1), 32-37.
92. Bhattacharyya, S.; Akhgar, G.; Gebert, M.; Karel, J.; Edmonds, M. T.; Fuhrer, M. S. Recent Progress in Proximity Coupling of Magnetism to Topological Insulators. *Adv. Mater.* **2021,** 33, (33), 2007795.
93. Kou, X. F.; Jiang, W. J.; Lang, M. R.; Xiu, F. X.; He, L.; Wang, Y.; Wang, Y.; Yu, X. X.; Fedorov, A. V.; Zhang, P.; Wang, K. L. Magnetically doped semiconducting topological insulators. *J. Appl. Phys.* **2012,** 112, (6), 063912.
94. Li, W.; Claassen, M.; Chang, C.-Z.; Moritz, B.; Jia, T.; Zhang, C.; Rebec, S.; Lee, J. J.; Hashimoto, M.; Lu, D. H.; Moore, R. G.; Moodera, J. S.; Devereaux, T. P.; Shen, Z. X. Origin of the low critical observing temperature of the quantum anomalous Hall effect in V-doped (Bi, Sb)2Te3 film. *Sci. Rep.* **2016,** 6, (1), 32732.
95. Schmidt, T. M.; Miwa, R. H.; Fazzio, A. Spin texture and magnetic anisotropy of Co impurities in Bi_2Se_3 topological insulators. *Phys. Rev. B* **2011,** 84, (24), 245418.
96. Jin, K.-H.; Jhi, S.-H. Effect of atomic impurities on the helical surface states of the topological insulator Bi_2Te_3. *J. Phys.: Condens. Matter.* **2012,** 24, (17), 175001.
97. Li, Z. L.; Yang, J. H.; Chen, G. H.; Whangbo, M. H.; Xiang, H. J.; Gong, X. G. Strong single-ion anisotropy and anisotropic interactions of magnetic adatoms induced by topological surface states. *Phys. Rev. B* **2012,** 85, (5), 054426.
98. Mahani, M. R.; Pertsova, A.; Islam, M. F.; Canali, C. M. Interplay between Mn-acceptor state and Dirac surface states in Mn-doped Bi_2Se_3 topological insulator. *Phys. Rev. B* **2014,** 90, (19), 195441.
99. Eremeev, S. V.; Men'shov, V. N.; Tugushev, V. V.; Echenique, P. M.; Chulkov, E. V. Magnetic proximity effect at the three-dimensional topological insulator/magnetic insulator interface. *Phys. Rev. B* **2013,** 88, (14), 144430.
100. Lee, A. T.; Han, M. J.; Park, K. Magnetic proximity effect and spin-orbital texture at the Bi_2Se_3/EuS interface. *Phys. Rev. B* **2014,** 90, (15), 155103.
101. Zhang, J.; Velev, J. P.; Dang, X.; Tsymbal, E. Y. Band structure and spin texture of Bi_2Se_3 3*d* ferromagnetic metal interface. *Phys. Rev. B* **2016,** 94, (1), 014435.
102. Kim, J.; Kim, K.-W.; Wang, H.; Sinova, J.; Wu, R. Understanding the Giant Enhancement of Exchange Interaction in Bi_2Se_3-EuS Heterostructures. *Phys. Rev. Lett.* **2017,** 119, (2), 027201.
103. Eremeev, S. V.; Otrokov, M. M.; Chulkov, E. V. New Universal Type of Interface in the Magnetic Insulator/Topological Insulator Heterostructures. *Nano Lett.* **2018,** 18, (10), 6521-6529.
104. Hou, Y.; Kim, J.; Wu, R. Magnetizing topological surface states of Bi_2Se_3 with a CrI_3

monolayer. *Sci. Adv.* **2019,** 5, (5), eaaw1874.
105. Fan, Y.; Kou, X.; Upadhyaya, P.; Shao, Q.; Pan, L.; Lang, M.; Che, X.; Tang, J.; Montazeri, M.; Murata, K.; Chang, L.-T.; Akyol, M.; Yu, G.; Nie, T.; Wong, K. L.; Liu, J.; Wang, Y.; Tserkovnyak, Y.; Wang, K. L. Electric-field control of spin–orbit torque in a magnetically doped topological insulator. *Nat. Nanotechnol.* **2016,** 11, (4), 352-359.
106. Ye, M.; Li, W.; Zhu, S.; Takeda, Y.; Saitoh, Y.; Wang, J.; Pan, H.; Nurmamat, M.; Sumida, K.; Ji, F.; Liu, Z.; Yang, H.; Liu, Z.; Shen, D.; Kimura, A.; Qiao, S.; Xie, X. Carrier-mediated ferromagnetism in the magnetic topological insulator Cr-doped $(Sb,Bi)_2Te_3$. *Nat. Commun.* **2015,** 6, (1), 8913.
107. Miron, I. M.; Garello, K.; Gaudin, G.; Zermatten, P.-J.; Costache, M. V.; Auffret, S.; Bandiera, S.; Rodmacq, B.; Schuhl, A.; Gambardella, P. Perpendicular switching of a single ferromagnetic layer induced by in-plane current injection. *Nature* **2011,** 476, (7359), 189-193.
108. Liu, L.; Pai, C.-F.; Li, Y.; Tseng, H. W.; Ralph, D. C.; Buhrman, R. A. Spin-Torque Switching with the Giant Spin Hall Effect of Tantalum. *Science* **2012,** 336, (6081), 555-558.
109. Garello, K.; Miron, I. M.; Avci, C. O.; Freimuth, F.; Mokrousov, Y.; Blügel, S.; Auffret, S.; Boulle, O.; Gaudin, G.; Gambardella, P. Symmetry and magnitude of spin–orbit torques in ferromagnetic heterostructures. *Nat. Nanotech.* **2013,** 8, (8), 587-593.
110. Wang, Y.; Deorani, P.; Banerjee, K.; Koirala, N.; Brahlek, M.; Oh, S.; Yang, H. Topological Surface States Originated Spin-Orbit Torques in Bi_2Se_3. *Phys. Rev. Lett.* **2015,** 114, (25), 257202.
111. Rojas-Sánchez, J. C.; Oyarzún, S.; Fu, Y.; Marty, A.; Vergnaud, C.; Gambarelli, S.; Vila, L.; Jamet, M.; Ohtsubo, Y.; Taleb-Ibrahimi, A.; Le Fèvre, P.; Bertran, F.; Reyren, N.; George, J. M.; Fert, A. Spin to Charge Conversion at Room Temperature by Spin Pumping into a New Type of Topological Insulator: α-Sn Films. *Phys. Rev. Lett.* **2016,** 116, (9), 096602.
112. Kondou, K.; Yoshimi, R.; Tsukazaki, A.; Fukuma, Y.; Matsuno, J.; Takahashi, K. S.; Kawasaki, M.; Tokura, Y.; Otani, Y. Fermi-level-dependent charge-to-spin current conversion by Dirac surface states of topological insulators. *Nat. Phys.* **2016,** 12, (11), 1027-1031.
113. Wu, H.; Chen, A.; Zhang, P.; He, H.; Nance, J.; Guo, C.; Sasaki, J.; Shirokura, T.; Hai, P. N.; Fang, B.; Razavi, S. A.; Wong, K.; Wen, Y.; Ma, Y.; Yu, G.; Carman, G. P.; Han, X.; Zhang, X.; Wang, K. L. Magnetic memory driven by topological insulators. *Nat. Commun.* **2021,** 12, (1), 6251.
114. Hull, D.; Bacon, D. J., *Introduction to Dislocations*. 5 ed.; Butterworth-Heinemann, Oxford: 2011.
115. Ng, H. M.; Doppalapudi, D.; Moustakas, T. D.; Weimann, N. G.; Eastman, L. F. The role of dislocation scattering in n-type GaN films. *Appl. Phys. Lett.* **1998,** 73, (6), 821-823.
116. Look, D. C.; Sizelove, J. R. Dislocation Scattering in GaN. *Phys. Rev. Lett.* **1999,** 82, (6), 1237-1240.
117. Ross, F. M.; Hull, R.; Bahnck, D.; Bean, J. C.; Peticolas, L. J.; King, C. A. Changes in electrical device characteristics during the in situ formation of dislocations. *Appl. Phys. Lett.* **1993,** 62, (12), 1426-1428.
118. Giovane, L. M.; Luan, H.-C.; Agarwal, A. M.; Kimerling, L. C. Correlation between leakage current density and threading dislocation density in SiGe p-i-n diodes grown on relaxed graded buffer layers. *Appl. Phys. Lett.* **2001,** 78, (4), 541-543.
119. Eaglesham, D. J.; Cerullo, M. Dislocation-free Stranski-Krastanow growth of Ge on Si(100). *Phys. Rev. Lett.* **1990,** 64, (16), 1943-1946.

120. Ran, Y.; Zhang, Y.; Vishwanath, A. One-dimensional topologically protected modes in topological insulators with lattice dislocations. *Nat. Phys.* **2009,** 5, (4), 298-303.
121. Slager, R.-J.; Mesaros, A.; Juričić, V.; Zaanen, J. Interplay between electronic topology and crystal symmetry: Dislocation-line modes in topological band insulators. *Phys. Rev. B* **2014,** 90, (24), 241403.
122. Teo, J. C. Y.; Hughes, T. L. Topological Defects in Symmetry-Protected Topological Phases. *Annu. Rev. Condens. Matter Phys.* **2017,** 8, (1), 211-237.
123. Hu, L.; Huang, H.; Wang, Z.; Jiang, W.; Ni, X.; Zhou, Y.; Zielasek, V.; Lagally, M. G.; Huang, B.; Liu, F. Ubiquitous Spin-Orbit Coupling in a Screw Dislocation with High Spin Coherency. *Phys. Rev. Lett.* **2018,** 121, (6), 066401.
124. Li, X.; Zhang, S.; Huang, H.; Hu, L.; Liu, F.; Wang, Q. Unidirectional Spin–Orbit Interaction Induced by the Line Defect in Monolayer Transition Metal Dichalcogenides for High-Performance Devices. *Nano Lett.* **2019,** 19, (9), 6005-6012.
125. Rashba, E. I. Properties of semiconductors with an extremum loop. I. Cyclotron and combinational resonance in a magnetic field perpendicular to the plane of the loop. *Sov. Phys. Solid State* **1960,** 2, 1109-1122.
126. Dresselhaus, G. Spin-Orbit Coupling Effects in Zinc Blende Structures. *Phys. Rev.* **1955,** 100, (2), 580-586.
127. Schliemann, J.; Egues, J. C.; Loss, D. Nonballistic Spin-Field-Effect Transistor. *Phys. Rev. Lett.* **2003,** 90, (14), 146801.
128. Bernevig, B. A.; Orenstein, J.; Zhang, S.-C. Exact SU(2) Symmetry and Persistent Spin Helix in a Spin-Orbit Coupled System. *Phys. Rev. Lett.* **2006,** 97, (23), 236601.
129. Lin, Z.; Carvalho, B. R.; Kahn, E.; Lv, R.; Rao, R.; Terrones, H.; Pimenta, M. A.; Terrones, M. Defect engineering of two-dimensional transition metal dichalcogenides. *2D Mater.* **2016,** 3, (2), 022002.
130. Chuang, P.; Ho, S.-C.; Smith, L. W.; Sfigakis, F.; Pepper, M.; Chen, C.-H.; Fan, J.-C.; Griffiths, J. P.; Farrer, I.; Beere, H. E.; Jones, G. A. C.; Ritchie, D. A.; Chen, T.-M. All-electric all-semiconductor spin field-effect transistors. *Nat. Nanotech.* **2015,** 10, (1), 35-39.
131. Datta, S.; Das, B. Electronic analog of the electro-optic modulator. *Appl. Phys. Lett.* **1990,** 56, (7), 665-667.
132. Koralek, J. D.; Weber, C. P.; Orenstein, J.; Bernevig, B. A.; Zhang, S.-C.; Mack, S.; Awschalom, D. D. Emergence of the persistent spin helix in semiconductor quantum wells. *Nature* **2009,** 458, (7238), 610-613.
133. Pan, Y.; Zhou, J. Toggling Valley-Spin Locking and Nonlinear Optical Properties of Single-Element Multiferroic Monolayers via Light. *Phys. Rev. Appl.* **2020,** 14, (1), 014024.
134. Jin, K.-H.; Oh, E.; Stania, R.; Liu, F.; Yeom, H. W. Enhanced Berry Curvature Dipole and Persistent Spin Texture in the Bi(110) Monolayer. *Nano Lett.* **2021,** 21, (22), 9468-9475.
135. Tao, L. L.; Tsymbal, E. Y. Persistent spin texture enforced by symmetry. *Nat. Commun.* **2018,** 9, (1), 2763.
136. Tao, L. L.; Tsymbal, E. Y. Perspectives of spin-textured ferroelectrics. *J. Phys. D: Appl. Phys.* **2021,** 54, (11), 113001.
137. Kim, J.; Kim, K.-W.; Shin, D.; Lee, S.-H.; Sinova, J.; Park, N.; Jin, H. Prediction of ferroelectricity-driven Berry curvature enabling charge- and spin-controllable photocurrent in tin telluride monolayers. *Nat. Commun.* **2019,** 10, (1), 3965.
138. Lee, H.; Im, J.; Jin, H. Emergence of the giant out-of-plane Rashba effect and tunable

nanoscale persistent spin helix in ferroelectric SnTe thin films. *Appl. Phys. Lett.* **2020,** 116, (2), 022411.
139. Sławińska, J.; Cerasoli, F. T.; Gopal, P.; Costa, M.; Curtarolo, S.; Buongiorno Nardelli, M. Ultrathin SnTe films as a route towards all-in-one spintronics devices. *2D Mater.* **2020,** 7, (2), 025026.
140. Moore, J. E. The birth of topological insulators. *Nature* **2010,** 464, (7286), 194-198.
141. (IEEE), I. o. E. a. E. E., International Roadmap for Devices and Systems (IRDS™) 2021 Edition. 2021.
142. Thomas, S. Gate-all-around transistors stack up. *Nat. Electron.* **2020,** 3, (12), 728-728.
143. Wang, X.; Zidan, M. A.; Lu, W. D. A Crossbar-Based In-Memory Computing Architecture. *IEEE Transactions on Circuits and Systems I: Regular Papers* **2020,** 67, (12), 4224-4232.
144. Karl, N. Charge carrier transport in organic semiconductors. *Synthetic Metals* **2003,** 133-134, 649-657.
145. Jiang, W.; Zhou, M.; Liu, Z.; Sun, D.; Vardeny, Z. V.; Liu, F. Structural, electronic, and magnetic properties of tris(8-hydroxyquinoline)iron(III) molecules and their magnetic coupling with ferromagnetic surface: first-principles study. *J. Phys.: Condens. Matter.* **2016,** 28, (17), 176004.
146. Sun, X.; Wu, K.-H.; Sakamoto, R.; Kusamoto, T.; Maeda, H.; Ni, X.; Jiang, W.; Liu, F.; Sasaki, S.; Masunaga, H.; Nishihara, H. Bis(aminothiolato)nickel nanosheet as a redox switch for conductivity and an electrocatalyst for the hydrogen evolution reaction. *Chem. Sci.* **2017,** 8, (12), 8078-8085.
147. Shu-Yau, W. A new ferroelectric memory device, metal-ferroelectric-semiconductor transistor. *IEEE Trans. Electron Devices* **1974,** 21, (8), 499-504.
148. Si, M.; Saha, A. K.; Gao, S.; Qiu, G.; Qin, J.; Duan, Y.; Jian, J.; Niu, C.; Wang, H.; Wu, W.; Gupta, S. K.; Ye, P. D. A ferroelectric semiconductor field-effect transistor. *Nat. Electron.* **2019,** 2, (12), 580-586.
149. Xu, K.; Jiang, W.; Gao, X.; Zhao, Z.; Low, T.; Zhu, W. Optical control of ferroelectric switching and multifunctional devices based on van der Waals ferroelectric semiconductors. *Nanoscale* **2020,** 12, (46), 23488-23496.
150. Yang, A.; Blancon, J.-C.; Jiang, W.; Zhang, H.; Wong, J.; Yan, E.; Lin, Y.-R.; Crochet, J.; Kanatzidis, M. G.; Jariwala, D.; Low, T.; Mohite, A. D.; Atwater, H. A. Giant Enhancement of Photoluminescence Emission in WS_2-Two-Dimensional Perovskite Heterostructures. *Nano Lett.* **2019,** 19, (8), 4852-4860.
151. Wang, L.; Meric, I.; Huang, P. Y.; Gao, Q.; Gao, Y.; Tran, H.; Taniguchi, T.; Watanabe, K.; Campos, L. M.; Muller, D. A.; Guo, J.; Kim, P.; Hone, J.; Shepard, K. L.; Dean, C. R. One-Dimensional Electrical Contact to a Two-Dimensional Material. *Science* **2013,** 342, (6158), 614-617.
152. Roy, T.; Tosun, M.; Kang, J. S.; Sachid, A. B.; Desai, S. B.; Hettick, M.; Hu, C. C.; Javey, A. Field-Effect Transistors Built from All Two-Dimensional Material Components. *ACS Nano* **2014,** 8, (6), 6259-6264.
153. Gilbert, M. J. Topological electronics. *Commun. Phys.* **2021,** 4, (1), 70.
154. Seidel, J. Nanoelectronics based on topological structures. *Nat. Mater.* **2019,** 18, (3), 188-190.
155. Jiang, W.; Liu, Z.; Mei, J.-W.; Cui, B.; Liu, F. Dichotomy between frustrated local spins and conjugated electrons in a two-dimensional metal–organic framework. *Nanoscale* **2019,** 11, (3), 955-961.

156. Torsi, L.; Magliulo, M.; Manoli, K.; Palazzo, G. Organic field-effect transistor sensors: a tutorial review. *Chem. Soc. Rev.* **2013,** 42, (22), 8612-8628.
157. Reddy, N. N.; Panda, D. K. A Comprehensive Review on Tunnel Field-Effect Transistor (TFET) Based Biosensors: Recent Advances and Future Prospects on Device Structure and Sensitivity. *Silicon* **2021,** 13, (9), 3085-3100.
158. Ferain, I.; Colinge, C. A.; Colinge, J.-P. Multigate transistors as the future of classical metal–oxide–semiconductor field-effect transistors. *Nature* **2011,** 479, (7373), 310-316.
159. Ando, Y. Topological Insulator Materials. *J. Phys. Soc. Jpn.* **2013,** 82, (10), 102001.
160. Fu, L.; Kane, C. L.; Mele, E. J. Topological Insulators in Three Dimensions. *Phys. Rev. Lett.* **2007,** 98, (10), 106803.
161. Vergniory, M. G.; Elcoro, L.; Felser, C.; Regnault, N.; Bernevig, B. A.; Wang, Z. A complete catalogue of high-quality topological materials. *Nature* **2019,** 566, (7745), 480-485.
162. Xu, Y.; Elcoro, L.; Song, Z.-D.; Wieder, B. J.; Vergniory, M. G.; Regnault, N.; Chen, Y.; Felser, C.; Bernevig, B. A. High-throughput calculations of magnetic topological materials. *Nature* **2020,** 586, (7831), 702-707.
163. Jiang, W.; de Sousa, D. J. P.; Wang, J.-P.; Low, T. Giant Anomalous Hall Effect due to Double-Degenerate Quasiflat Bands. *Phys. Rev. Lett.* **2021,** 126, (10), 106601.
164. Jiang, W.; Zhang, S.; Wang, Z.; Liu, F.; Low, T. Topological Band Engineering of Lieb Lattice in Phthalocyanine-Based Metal–Organic Frameworks. *Nano Lett.* **2020,** 20, (3), 1959-1966.
165. Jiang, W.; Liu, F., Organic Topological Insulators. In *World Scientific Reference on Spin in Organics*, WORLD SCIENTIFIC: 2017; pp 201-224.
166. Jiang, W.; Huang, H.; Liu, F.; Wang, J.-P.; Low, T. Magnetic Weyl semimetals with diamond structure realized in spinel compounds. *Phys. Rev. B* **2020,** 101, (12), 121113.
167. Zhang, W.; Yu, R.; Zhang, H.-J.; Dai, X.; Fang, Z. First-principles studies of the three-dimensional strong topological insulators Bi_2Te_3, Bi_2Se_3 and Sb_2Te_3. *New J. Phys.* **2010,** 12, (6), 065013.
168. Zhang, Y.; He, K.; Chang, C.-Z.; Song, C.-L.; Wang, L.-L.; Chen, X.; Jia, J.-F.; Fang, Z.; Dai, X.; Shan, W.-Y.; Shen, S.-Q.; Niu, Q.; Qi, X.-L.; Zhang, S.-C.; Ma, X.-C.; Xue, Q.-K. Crossover of the three-dimensional topological insulator Bi_2Se_3 to the two-dimensional limit. *Nat. Phys.* **2010,** 6, (8), 584-588.
169. Kim, D.; Cho, S.; Butch, N. P.; Syers, P.; Kirshenbaum, K.; Adam, S.; Paglione, J.; Fuhrer, M. S. Surface conduction of topological Dirac electrons in bulk insulating Bi_2Se_3. *Nat. Phys.* **2012,** 8, (6), 459-463.
170. Steinberg, H.; Gardner, D. R.; Lee, Y. S.; Jarillo-Herrero, P. Surface State Transport and Ambipolar Electric Field Effect in Bi_2Se_3 Nanodevices. *Nano Lett.* **2010,** 10, (12), 5032-5036.
171. Liu, H.; Ye, P. D. Atomic-layer-deposited Al_2O_3 on Bi_2Te_3 for topological insulator field-effect transistors. *Appl. Phys. Lett.* **2011,** 99, (5), 052108.
172. Hor, Y. S.; Richardella, A.; Roushan, P.; Xia, Y.; Checkelsky, J. G.; Yazdani, A.; Hasan, M. Z.; Ong, N. P.; Cava, R. J. *p*-type Bi_2Se_3 for topological insulator and low-temperature thermoelectric applications. *Phys. Rev. B* **2009,** 79, (19), 195208.
173. Checkelsky, J. G.; Hor, Y. S.; Cava, R. J.; Ong, N. P. Bulk Band Gap and Surface State Conduction Observed in Voltage-Tuned Crystals of the Topological Insulator Bi_2Se_3. *Phys. Rev. Lett.* **2011,** 106, (19), 196801.
174. Kong, D.; Chen, Y.; Cha, J. J.; Zhang, Q.; Analytis, J. G.; Lai, K.; Liu, Z.; Hong, S. S.; Koski,

K. J.; Mo, S.-K.; Hussain, Z.; Fisher, I. R.; Shen, Z.-X.; Cui, Y. Ambipolar field effect in the ternary topological insulator $(Bi_xSb_{1-x})_2Te_3$ by composition tuning. *Nat. Nanotechnol.* **2011,** 6, (11), 705-709.

175. Cho, S.; Butch, N. P.; Paglione, J.; Fuhrer, M. S. Insulating Behavior in Ultrathin Bismuth Selenide Field Effect Transistors. *Nano Lett.* **2011,** 11, (5), 1925-1927.
176. Chang, J.; Register, L. F.; Banerjee, S. K. Topological insulator Bi_2Se_3 thin films as an alternative channel material in metal-oxide-semiconductor field-effect transistors. *J. Appl. Phys.* **2012,** 112, (12), 124511.
177. Lu, H.-Z.; Shan, W.-Y.; Yao, W.; Niu, Q.; Shen, S.-Q. Massive Dirac fermions and spin physics in an ultrathin film of topological insulator. *Phys. Rev. B* **2010,** 81, (11), 115407.
178. Liu, C.-X.; Zhang, H.; Yan, B.; Qi, X.-L.; Frauenheim, T.; Dai, X.; Fang, Z.; Zhang, S.-C. Oscillatory crossover from two-dimensional to three-dimensional topological insulators. *Phys. Rev. B* **2010,** 81, (4), 041307.
179. Linder, J.; Yokoyama, T.; Sudbø, A. Anomalous finite size effects on surface states in the topological insulator Bi_2Se_3. *Phys. Rev. B* **2009,** 80, (20), 205401.
180. Qian, X.; Liu, J.; Fu, L.; Li, J. Quantum spin Hall effect in two-dimensional transition metal dichalcogenides. *Science* **2014,** 346, (6215), 1344-1347.
181. Vandenberghe, W. G.; Fischetti, M. V. Imperfect two-dimensional topological insulator field-effect transistors. *Nat. Commun.* **2017,** 8, (1), 14184.
182. Li, X.; Liu, F. Topological field-effect transistor with quantized on/off conductance of helical/chiral dislocation states. *Phys. Rev. B* **2023,** 107, (22), 224101.
183. Liu, J.; Hsieh, T. H.; Wei, P.; Duan, W.; Moodera, J.; Fu, L. Spin-filtered edge states with an electrically tunable gap in a two-dimensional topological crystalline insulator. *Nat. Mater.* **2014,** 13, (2), 178-183.
184. Hu, G.; Zhang, Y.; Li, L.; Wang, Z. L. Piezotronic Transistor Based on Topological Insulators. *ACS Nano* **2018,** 12, (1), 779-785.
185. Collins, J. L.; Tadich, A.; Wu, W.; Gomes, L. C.; Rodrigues, J. N. B.; Liu, C.; Hellerstedt, J.; Ryu, H.; Tang, S.; Mo, S.-K.; Adam, S.; Yang, S. A.; Fuhrer, M. S.; Edmonds, M. T. Electric-field-tuned topological phase transition in ultrathin Na_3Bi. *Nature* **2018,** 564, (7736), 390-394.
186. Niu, C.; Buhl, P. M.; Bihlmayer, G.; Wortmann, D.; Dai, Y.; Blügel, S.; Mokrousov, Y. Robust dual topological character with spin-valley polarization in a monolayer of the Dirac semimetal Na_3Bi. *Phys. Rev. B* **2017,** 95, (7), 075404.
187. Pan, H.; Wu, M.; Liu, Y.; Yang, S. A. Electric control of topological phase transitions in Dirac semimetal thin films. *Sci. Rep.* **2015,** 5, (1), 14639.
188. Wang, J.; Li, W.; Cheng, P.; Song, C.; Zhang, T.; Deng, P.; Chen, X.; Ma, X.; He, K.; Jia, J.-F.; Xue, Q.-K.; Zhu, B.-F. Power-law decay of standing waves on the surface of topological insulators. *Phys. Rev. B* **2011,** 84, (23), 235447.
189. Wang, J.; Chen, X.; Zhu, B.-F.; Zhang, S.-C. Topological p-n junction. *Phys. Rev. B* **2012,** 85, (23), 235131.
190. Eschbach, M.; Młyńczak, E.; Kellner, J.; Kampmeier, J.; Lanius, M.; Neumann, E.; Weyrich, C.; Gehlmann, M.; Gospodarič, P.; Döring, S.; Mussler, G.; Demarina, N.; Luysberg, M.; Bihlmayer, G.; Schäpers, T.; Plucinski, L.; Blügel, S.; Morgenstern, M.; Schneider, C. M.; Grützmacher, D. Realization of a vertical topological p–n junction in epitaxial Sb_2Te_3/Bi_2Te_3 heterostructures. *Nat. Commun.* **2015,** 6, (1), 8816.
191. Young, A. F.; Kim, P. Quantum interference and Klein tunnelling in graphene heterojunctions.

Nat. Phys. **2009,** 5, (3), 222-226.
192. Habib, K. M. M.; Sajjad, R. N.; Ghosh, A. W. Chiral Tunneling of Topological States: Towards the Efficient Generation of Spin Current Using Spin-Momentum Locking. *Phys. Rev. Lett.* **2015,** 114, (17), 176801.
193. Ilan, R.; de Juan, F.; Moore, J. E. Spin-Based Mach-Zehnder Interferometry in Topological Insulator p-n Junctions. *Phys. Rev. Lett.* **2015,** 115, (9), 096802.
194. Tu, N. H.; Tanabe, Y.; Satake, Y.; Huynh, K. K.; Tanigaki, K. In-plane topological p-n junction in the three-dimensional topological insulator $Bi_{2-x}Sb_xTe_{3-y}Se_y$. *Nat. Commun.* **2016,** 7, (1), 13763.
195. Kim, S. H.; Jin, K.-H.; Kho, B. W.; Park, B.-G.; Liu, F.; Kim, J. S.; Yeom, H. W. Atomically Abrupt Topological p–n Junction. *ACS Nano* **2017,** 11, (10), 9671-9677.
196. Gupta, G.; Jalil, M. B. A.; Liang, G. Evaluation of mobility in thin Bi_2Se_3 Topological Insulator for prospects of Local Electrical Interconnects. *Sci. Rep.* **2014,** 4, (1), 6838.
197. Boutin, S.; Lopes, P. L. S.; Mu, A.; Mendes, U. C.; Garate, I. Topological Josephson bifurcation amplifier: Semiclassical theory. *J. Appl. Phys.* **2021,** 129, (21), 214302.
198. Chen, J.; Zhang, T.; Wang, J.; Zhang, N.; Ji, W.; Zhou, S.; Chai, Y. Field-Effect Chiral Anomaly Devices with Dirac Semimetal. *Adv. Funct. Mater.* **2021,** 31, (40), 2104192.
199. Zhao, B.; Khokhriakov, D.; Zhang, Y.; Fu, H.; Karpiak, B.; Hoque, A. M.; Xu, X.; Jiang, Y.; Yan, B.; Dash, S. P. Observation of charge to spin conversion in Weyl semimetal ${\mathrm{WTe}}_{2}$ at room temperature. *Phys. Rev. Res.* **2020,** 2, (1), 013286.
200. Ohnishi, K.; Aoki, M.; Ohshima, R.; Shigematsu, E.; Ando, Y.; Takenobu, T.; Shiraishi, M. All-Electric Spin Device Operation Using the Weyl Semimetal, WTe2, at Room Temperature. *Adv. Electron. Mater.* **2023,** 9, (1), 2200647.
201. Budich, J. C.; Bergholtz, E. J. Non-Hermitian Topological Sensors. *Phys. Rev. Lett.* **2020,** 125, (18), 180403.
202. Politano, A.; Viti, L.; Vitiello, M. S. Optoelectronic devices, plasmonics, and photonics with topological insulators. *APL Materials* **2017,** 5, (3), 35504-35504.
203. Yue, Z.; Wang, X.; Gu, M., Topological Insulator Materials for Advanced Optoelectronic Devices. John Wiley & Sons, Ltd: 2019; pp 45-70.
204. Stauber, T.; Gómez-Santos, G.; Brey, L. Plasmonics in Topological Insulators: Spin–Charge Separation, the Influence of the Inversion Layer, and Phonon–Plasmon Coupling. *ACS Photonics* **2017,** 4, (12), 2978-2988.
205. Lu, L.; Joannopoulos, J. D.; Soljačić, M. Topological photonics. *Nat. Photon.* **2014,** 8, (11), 821-829.
206. Ozawa, T.; Price, H. M.; Amo, A.; Goldman, N.; Hafezi, M.; Lu, L.; Rechtsman, M. C.; Schuster, D.; Simon, J.; Zilberberg, O.; Carusotto, I. Topological photonics. *Rev. Mod. Phys.* **2019,** 91, (1), 015006.
207. Segev, M.; Bandres, M. A. Topological photonics: Where do we go from here? *Nanophotonics* **2020,** 10, (1), 425-434.
208. Vitale, S. A.; Nezich, D.; Varghese, J. O.; Kim, P.; Gedik, N.; Jarillo-Herrero, P.; Xiao, D.; Rothschild, M. Valleytronics: Opportunities, Challenges, and Paths Forward. *Small* **2018,** 14, (38), 1801483.
209. Xue, H.; Yang, Y.; Zhang, B. Topological Valley Photonics: Physics and Device Applications. *Adv. Photonics Res.* **2021,** 2, (8), 2100013.
210. Schaibley, J. R.; Yu, H.; Clark, G.; Rivera, P.; Ross, J. S.; Seyler, K. L.; Yao, W.; Xu, X.

Valleytronics in 2D materials. *Nat. Rev. Mater.* **2016,** 1, (11), 16055-16055.
211. Xu, X.; Yao, W.; Xiao, D.; Heinz, T. F. Spin and pseudospins in layered transition metal dichalcogenides. *Nat. Phys.* **2014,** 10, (5), 343-350.
212. Ju, L.; Shi, Z.; Nair, N.; Lv, Y.; Jin, C.; Velasco, J.; Ojeda-Aristizabal, C.; Bechtel, H. A.; Martin, M. C.; Zettl, A.; Analytis, J.; Wang, F. Topological valley transport at bilayer graphene domain walls. *Nature* **2015,** 520, (7549), 650-655.
213. Mak, K. F.; McGill, K. L.; Park, J.; McEuen, P. L. The valley Hall effect in MoS_2 transistors. *Science* **2014,** 344, (6191), 1489-1492.
214. Zeng, H.; Dai, J.; Yao, W.; Xiao, D.; Cui, X. Valley polarization in MoS_2 monolayers by optical pumping. *Nat. Nanotechnol.* **2012,** 7, (8), 490-493.
215. Mak, K. F.; He, K.; Shan, J.; Heinz, T. F. Control of valley polarization in monolayer MoS_2 by optical helicity. *Nat. Nanotech.* **2012,** 7, (8), 494-498.
216. Cao, T.; Wang, G.; Han, W.; Ye, H.; Zhu, C.; Shi, J.; Niu, Q.; Tan, P.; Wang, E.; Liu, B.; Feng, J. Valley-selective circular dichroism of monolayer molybdenum disulphide. *Nat. Commun.* **2012,** 3, (1), 887.
217. Chen, F.-W.; Lue, N.-Y.; Chou, M.-Y.; Wu, Y.-S. G. All-electrical valley filtering in graphene systems. I. A path to integrated electro-valleytronics. *J. Appl. Phys.* **2022,** 132, (16), 164303.
218. Rohling, N.; Russ, M.; Burkard, G. Hybrid Spin and Valley Quantum Computing with Singlet-Triplet Qubits. *Phys. Rev. Lett.* **2014,** 113, (17), 176801.
219. Wu, G. Y.; Lue, N. Y.; Chen, Y. C. Quantum manipulation of valleys in bilayer graphene. *Phys. Rev. B* **2013,** 88, (12), 125422.
220. Shimazaki, Y.; Yamamoto, M.; Borzenets, I. V.; Watanabe, K.; Taniguchi, T.; Tarucha, S. Generation and detection of pure valley current by electrically induced Berry curvature in bilayer graphene. *Nat. Phys.* **2015,** 11, (12), 1032-1036.
221. Rycerz, A.; Tworzydło, J.; Beenakker, C. W. J. Valley filter and valley valve in graphene. *Nat. Phys.* **2007,** 3, (3), 172-175.
222. Lee, M. K.; Lue, N. Y.; Wen, C. K.; Wu, G. Y. Valley-based field-effect transistors in graphene. *Phys. Rev. B* **2012,** 86, (16), 165411.
223. Ye, T.; Li, Y.; Li, J.; Shen, H.; Ren, J.; Ning, C.-Z.; Li, D. Nonvolatile electrical switching of optical and valleytronic properties of interlayer excitons. *Light Sci. Appl.* **2022,** 11, (1), 23.
224. Raghu, S.; Haldane, F. D. M. Analogs of quantum-Hall-effect edge states in photonic crystals. *Phys. Rev. A* **2008,** 78, (3), 033834.
225. Haldane, F. D. M.; Raghu, S. Possible Realization of Directional Optical Waveguides in Photonic Crystals with Broken Time-Reversal Symmetry. *Phys. Rev. Lett.* **2008,** 100, (1), 013904.
226. John, S. Strong localization of photons in certain disordered dielectric superlattices. *Phys. Rev. Lett.* **1987,** 58, (23), 2486-2489.
227. Yablonovitch, E. Inhibited Spontaneous Emission in Solid-State Physics and Electronics. *Phys. Rev. Lett.* **1987,** 58, (20), 2059-2062.
228. Khanikaev, A. B.; Hossein Mousavi, S.; Tse, W.-K.; Kargarian, M.; MacDonald, A. H.; Shvets, G. Photonic topological insulators. *Nat. Mater.* **2013,** 12, (3), 233-239.
229. Fang, K.; Yu, Z.; Fan, S. Realizing effective magnetic field for photons by controlling the phase of dynamic modulation. *Nat. Photon.* **2012,** 6, (11), 782-787.
230. Hafezi, M.; Demler, E. A.; Lukin, M. D.; Taylor, J. M. Robust optical delay lines with topological protection. *Nat. Phys.* **2011,** 7, (11), 907-912.

231. Wang, Z.; Chong, Y.; Joannopoulos, J. D.; Soljačić, M. Observation of unidirectional backscattering-immune topological electromagnetic states. *Nature* **2009,** 461, (7265), 772-775.
232. Wang, Z.; Chong, Y. D.; Joannopoulos, J. D.; Soljačić, M. Reflection-Free One-Way Edge Modes in a Gyromagnetic Photonic Crystal. *Phys. Rev. Lett.* **2008,** 100, (1), 013905.
233. He, C.; Chen, X.-L.; Lu, M.-H.; Li, X.-F.; Wan, W.-W.; Qian, X.-S.; Yin, R.-C.; Chen, Y.-F. Tunable one-way cross-waveguide splitter based on gyromagnetic photonic crystal. *Appl. Phys. Lett.* **2010,** 96, (11), 111111.
234. Zang, X.; Jiang, C. Edge mode in nonreciprocal photonic crystal waveguide: manipulating the unidirectional electromagnetic pulse dynamically. *J. Opt. Soc. Am. B* **2011,** 28, (3), 554-557.
235. Fu, J.-X.; Liu, R.-J.; Li, Z.-Y. Robust one-way modes in gyromagnetic photonic crystal waveguides with different interfaces. *Appl. Phys. Lett.* **2010,** 97, (4), 041112.
236. Fu, J.-X.; Lian, J.; Liu, R.-J.; Gan, L.; Li, Z.-Y. Unidirectional channel-drop filter by one-way gyromagnetic photonic crystal waveguides. *Appl. Phys. Lett.* **2011,** 98, (21), 211104.
237. Qiu, W.; Wang, Z.; Soljačić, M. Broadband circulators based on directional coupling of one-way waveguides. *Opt. Express* **2011,** 19, (22), 22248-22257.
238. Yang, Y.; Poo, Y.; Wu, R.-x.; Gu, Y.; Chen, P. Experimental demonstration of one-way slow wave in waveguide involving gyromagnetic photonic crystals. *Appl. Phys. Lett.* **2013,** 102, (23), 231113.
239. Skirlo, S. A.; Lu, L.; Soljačić, M. Multimode One-Way Waveguides of Large Chern Numbers. *Phys. Rev. Lett.* **2014,** 113, (11), 113904.
240. Hafezi, M.; Mittal, S.; Fan, J.; Migdall, A.; Taylor, J. M. Imaging topological edge states in silicon photonics. *Nat. Photonics* **2013,** 7, (12), 1001-1005.
241. Rechtsman, M. C.; Zeuner, J. M.; Plotnik, Y.; Lumer, Y.; Podolsky, D.; Dreisow, F.; Nolte, S.; Segev, M.; Szameit, A. Photonic Floquet topological insulators. *Nature* **2013,** 496, (7444), 196-200.
242. Chen, W.-J.; Jiang, S.-J.; Chen, X.-D.; Zhu, B.; Zhou, L.; Dong, J.-W.; Chan, C. T. Experimental realization of photonic topological insulator in a uniaxial metacrystal waveguide. *Nat. Commun.* **2014,** 5, (1), 5782-5782.
243. Wu, L.-H.; Hu, X. Scheme for Achieving a Topological Photonic Crystal by Using Dielectric Material. *Phys. Rev. Lett.* **2015,** 114, (22), 223901-223901.
244. Ma, T.; Shvets, G. All-Si valley-Hall photonic topological insulator. *New J. Phys.* **2016,** 18, (2), 25012-25012.
245. Wang, Y. H.; Steinberg, H.; Jarillo-Herrero, P.; Gedik, N. Observation of Floquet-Bloch States on the Surface of a Topological Insulator. *Science* **2013,** 342, (6157), 453-457.
246. Maczewsky, L. J.; Zeuner, J. M.; Nolte, S.; Szameit, A. Observation of photonic anomalous Floquet topological insulators. *Nat. Commun.* **2017,** 8, (1), 13756-13756.
247. Mukherjee, S.; Spracklen, A.; Valiente, M.; Andersson, E.; Öhberg, P.; Goldman, N.; Thomson, R. R. Experimental observation of anomalous topological edge modes in a slowly driven photonic lattice. *Nat. Commun.* **2017,** 8, (1), 13918-13918.
248. Wintersperger, K.; Braun, C.; Ünal, F. N.; Eckardt, A.; Liberto, M. D.; Goldman, N.; Bloch, I.; Aidelsburger, M. Realization of an anomalous Floquet topological system with ultracold atoms. *Nat. Phys.* **2020,** 16, (10), 1058-1063.
249. Stützer, S.; Plotnik, Y.; Lumer, Y.; Titum, P.; Lindner, N. H.; Segev, M.; Rechtsman, M. C.; Szameit, A. Photonic topological Anderson insulators. *Nature* **2018,** 560, (7719), 461-465.
250. Yang, Z.; Lustig, E.; Lumer, Y.; Segev, M. Photonic Floquet topological insulators in a fractal

lattice. *Light: Science & Applications* **2020,** 9, (1), 128-128.
251. Liang, G. Q.; Chong, Y. D. Optical Resonator Analog of a Two-Dimensional Topological Insulator. *Phys. Rev. Lett.* **2013,** 110, (20), 203904-203904.
252. Chong, Y. Photonic insulators with a twist. *Nature* **2013,** 496, (7444), 173-174.
253. Harari, G.; Bandres, M. A.; Lumer, Y.; Rechtsman, M. C.; Chong, Y. D.; Khajavikhan, M.; Christodoulides, D. N.; Segev, M. Topological insulator laser: Theory. *Science* **2018,** 359, (6381).
254. Bandres, M. A.; Wittek, S.; Harari, G.; Parto, M.; Ren, J.; Segev, M.; Christodoulides, D. N.; Khajavikhan, M. Topological insulator laser: Experiments. *Science* **2018,** 359, (6381).
255. Amelio, I.; Carusotto, I. Theory of the Coherence of Topological Lasers. *Phys. Rev. X* **2020,** 10, (4), 41060-41060.
256. Zeng, Y.; Chattopadhyay, U.; Zhu, B.; Qiang, B.; Li, J.; Jin, Y.; Li, L.; Davies, A. G.; Linfield, E. H.; Zhang, B.; Chong, Y.; Wang, Q. J. Electrically pumped topological laser with valley edge modes. *Nature* **2020,** 578, (7794), 246-250.
257. Shao, Z.-K.; Chen, H.-Z.; Wang, S.; Mao, X.-R.; Yang, Z.-Q.; Wang, S.-L.; Wang, X.-X.; Hu, X.; Ma, R.-M. A high-performance topological bulk laser based on band-inversion-induced reflection. *Nat. Nanotechnol.* **2020,** 15, (1), 67-72.
258. Liu, Y. G.; Jung, P.; Parto, M.; Hayenga, W. E.; Christodoulides, D. N.; Khajavikhan, M. In *Towards the experimental demonstration of topological Haldane lattice in microring laser arrays (Conference Presentation)*, 2020, Belyanin, A. A.; Smowton, P. M., Eds. SPIE: pp 36-36.
259. Yang, Z.; Lustig, E.; Harari, G.; Plotnik, Y.; Lumer, Y.; Bandres, M. A.; Segev, M. Mode-Locked Topological Insulator Laser Utilizing Synthetic Dimensions. *Phys. Rev. X* **2020,** 10, (1), 11059-11059.
260. Yang, Y.; Yamagami, Y.; Yu, X.; Pitchappa, P.; Webber, J.; Zhang, B.; Fujita, M.; Nagatsuma, T.; Singh, R. Terahertz topological photonics for on-chip communication. *Nat. Photon.* **2020,** 14, (7), 446-451.
261. Maier, S. A., *Plasmonics: Fundamentals and Applications*. Springer US: 2007.
262. Fang, Z.; Zhu, X. Plasmonics in Nanostructures. *Adv. Mater.* **2013,** 25, (28), 3840-3856.
263. Stauber, T.; Gómez-Santos, G.; Brey, L. Spin-charge separation of plasmonic excitations in thin topological insulators. *Phys. Rev. B* **2013,** 88, (20), 205427-205427.
264. Politano, A.; Silkin, V. M.; Nechaev, I. A.; Vitiello, M. S.; Viti, L.; Aliev, Z. S.; Babanly, M. B.; Chiarello, G.; Echenique, P. M.; Chulkov, E. V. Interplay of Surface and Dirac Plasmons in Topological Insulators: The Case of Bi_2Te_3. *Phys. Rev. Lett.* **2015,** 115, (21), 216802-216802.
265. Zhang, Q.; Li, X.; Hossain, M. M.; Xue, Y.; Zhang, J.; Song, J.; Liu, J.; Turner, M. D.; Fan, S.; Bao, Q.; Gu, M. Graphene surface plasmons at the near-infrared optical regime. *Sci. Rep.* **2015,** 4, (1), 6559-6559.
266. Yuan, J.; Ma, W.; Zhang, L.; Lu, Y.; Zhao, M.; Guo, H.; Zhao, J.; Yu, W.; Zhang, Y.; Zhang, K.; Hoh, H. Y.; Li, X.; Loh, K. P.; Li, S.; Qiu, C.-W.; Bao, Q. Infrared Nanoimaging Reveals the Surface Metallic Plasmons in Topological Insulator. *ACS Photonics* **2017,** 4, (12), 3055-3062.
267. Di Pietro, P.; Ortolani, M.; Limaj, O.; Di Gaspare, A.; Giliberti, V.; Giorgianni, F.; Brahlek, M.; Bansal, N.; Koirala, N.; Oh, S.; Calvani, P.; Lupi, S. Observation of Dirac plasmons in a topological insulator. *Nat. Nanotechnol.* **2013,** 8, (8), 556-560.

268. Tan, C.; Yue, Z.; Dai, Z.; Bao, Q.; Wang, X.; Lu, H.; Wang, L. Nanograting-assisted generation of surface plasmon polaritons in Weyl semimetal WTe_2. *Optical Materials* **2018,** 86, 421-423.
269. Zhao, M.; Zhang, J.; Gao, N.; Song, P.; Bosman, M.; Peng, B.; Sun, B.; Qiu, C.-W.; Xu, Q.-H.; Bao, Q.; Loh, K. P. Actively Tunable Visible Surface Plasmons in Bi_2Te_3 and their Energy-Harvesting Applications. *Adv. Mater.* **2016,** 28, (16), 3138-3144.
270. Zhao, M.; Bosman, M.; Danesh, M.; Zeng, M.; Song, P.; Darma, Y.; Rusydi, A.; Lin, H.; Qiu, C.-W.; Loh, K. P. Visible Surface Plasmon Modes in Single Bi_2Te_3 Nanoplate. *Nano Lett.* **2015,** 15, (12), 8331-8335.
271. Dyakonov, M.; Shur, M. Shallow water analogy for a ballistic field effect transistor: New mechanism of plasma wave generation by dc current. *Phys. Rev. Lett.* **1993,** 71, (15), 2465-2468.
272. Tomadin, A.; Polini, M. Theory of the plasma-wave photoresponse of a gated graphene sheet. *Phys. Rev. B* **2013,** 88, (20), 205426-205426.
273. Konstantatos, G. Current status and technological prospect of photodetectors based on two-dimensional materials. *Nat. Commun.* **2018,** 9, (1), 5266-5266.
274. Viti, L.; Coquillat, D.; Politano, A.; Kokh, K. A.; Aliev, Z. S.; Babanly, M. B.; Tereshchenko, O. E.; Knap, W.; Chulkov, E. V.; Vitiello, M. S. Plasma-Wave Terahertz Detection Mediated by Topological Insulators Surface States. *Nano Lett.* **2016,** 16, (1), 80-87.
275. Wang, Z. F.; Liu, F. Self-Assembled Si(111) Surface States: 2D Dirac Material for THz Plasmonics. *Phys. Rev. Lett.* **2015,** 115, (2), 026803.
276. Wang, J.; Sui, X.; Gao, S.; Duan, W.; Liu, F.; Huang, B. Anomalous Dirac Plasmons in 1D Topological Electrides. *Phys. Rev. Lett.* **2019,** 123, (20), 206402.
277. Wang, J.; Sui, X.; Duan, W.; Liu, F.; Huang, B. Density-independent plasmons for terahertz-stable topological metamaterials. *Proc. Natl. Acad. Sci. USA* **2021,** 118, (19), e2023029118.
278. Burkov, A. A.; Hook, M. D.; Balents, L. Topological nodal semimetals. *Phys. Rev. B* **2011,** 84, (23), 235126.
279. Das Sarma, S.; Hwang, E. H. Collective Modes of the Massless Dirac Plasma. *Phys. Rev. Lett.* **2009,** 102, (20), 206412.
280. Shi, Z.; Hong, X.; Bechtel, H. A.; Zeng, B.; Martin, M. C.; Watanabe, K.; Taniguchi, T.; Shen, Y.-R.; Wang, F. Observation of a Luttinger-liquid plasmon in metallic single-walled carbon nanotubes. *Nat. Photon.* **2015,** 9, (8), 515-519.
281. Qi, X.-L.; Zhang, S.-C. Topological insulators and superconductors. *Rev. Mod. Phys.* **2011,** 83, (4), 1057-1110.
282. Raghu, S.; Chung, S. B.; Qi, X.-L.; Zhang, S.-C. Collective Modes of a Helical Liquid. *Phys. Rev. Lett.* **2010,** 104, (11), 116401-116401.
283. Agarwal, A.; Polini, M.; Vignale, G.; Flatté, M. E. Long-lived spin plasmons in a spin-polarized two-dimensional electron gas. *Phys. Rev. B* **2014,** 90, (15), 155409-155409.
284. Kogar, A.; Vig, S.; Thaler, A.; Wong, M. H.; Xiao, Y.; Reig-i-Plessis, D.; Cho, G. Y.; Valla, T.; Pan, Z.; Schneeloch, J.; Zhong, R.; Gu, G. D.; Hughes, T. L.; MacDougall, G. J.; Chiang, T. C.; Abbamonte, P. Surface Collective Modes in the Topological Insulators Bi_2Se_3 and $Bi_{0.5}Sb_{1.5}Te_{3-x}Se_x$. *Phys. Rev. Lett.* **2015,** 115, (25), 257402-257402.
285. Zhang, X.; Wang, J.; Zhang, S.-C. Topological insulators for high-performance terahertz to infrared applications. *Phys. Rev. B* **2010,** 82, (24), 245107-245107.
286. Yao, J.; Zheng, Z.; Yang, G. All-Layered 2D Optoelectronics: A High-Performance UV-vis-

NIR Broadband SnSe Photodetector with Bi_2Te_3 Topological Insulator Electrodes. *Adv. Funct. Mater.* **2017,** 27, (33), 1701823-1701823.

287. Gu, S.; Ding, K.; Pan, J.; Shao, Z.; Mao, J.; Zhang, X.; Jie, J. Self-driven, broadband and ultrafast photovoltaic detectors based on topological crystalline insulator SnTe/Si heterostructures. *J. Mater. Chem. A* **2017,** 5, (22), 11171-11178.
288. Sharma, A.; Senguttuvan, T. D.; Ojha, V. N.; Husale, S. Novel synthesis of topological insulator based nanostructures (Bi2Te3) demonstrating high performance photodetection. *Sci. Rep.* **2019,** 9, (1), 3804-3804.
289. Yao, J.; Zheng, Z.; Yang, G. Layered-material WS_2/topological insulator Bi_2Te_3 heterostructure photodetector with ultrahigh responsivity in the range from 370 to 1550 nm. *J. Mater. Chem. C* **2016,** 4, (33), 7831-7840.
290. Sharma, A.; Bhattacharyya, B.; Srivastava, A. K.; Senguttuvan, T. D.; Husale, S. High performance broadband photodetector using fabricated nanowires of bismuth selenide. *Sci. Rep.* **2016,** 6, (1), 19138-19138.
291. Salleo A, W. W. S., *Flexible Electronics*. Springer US: 2009; Vol. 11.
292. Gates, B. D. Flexible Electronics. *Science* **2009,** 323, (5921), 1566-1567.
293. Nathan, A.; Ahnood, A.; Cole, M. T.; Lee, S.; Suzuki, Y.; Hiralal, P.; Bonaccorso, F.; Hasan, T.; Garcia-Gancedo, L.; Dyadyusha, A.; Haque, S.; Andrew, P.; Hofmann, S.; Moultrie, J.; Chu, D.; Flewitt, A. J.; Ferrari, A. C.; Kelly, M. J.; Robertson, J.; Amaratunga, G. A. J.; Milne, W. I. Flexible Electronics: The Next Ubiquitous Platform. *Proceedings of the IEEE* **2012,** 100, (Special Centennial Issue), 1486-1517.
294. Gao, W.; Ota, H.; Kiriya, D.; Takei, K.; Javey, A. Flexible Electronics toward Wearable Sensing. *Acc. Chem. Res.* **2019,** 52, (3), 523-533.
295. Yang, Y.; Gao, W. Wearable and flexible electronics for continuous molecular monitoring. *Chem. Soc. Rev.* **2019,** 48, (6), 1465-1491.
296. Pandey, A.; Yadav, R.; Kaur, M.; Singh, P.; Gupta, A.; Husale, S. High performing flexible optoelectronic devices using thin films of topological insulator. *Sci. Rep.* **2021,** 11, (1), 832-832.
297. Bergholtz, E. J.; Liu, Z. Topological Flat Band Models and Fractional Chern Insulators. *Int. J. Mod. Phys. B* **2013,** 27, (24), 1330017-1330017.
298. Liu, T.; Repellin, C.; Bernevig, B. A.; Regnault, N. Fractional Chern insulators beyond Laughlin states. *Phys. Rev. B* **2013,** 87, (20), 205136-205136.
299. Li, W.; Liu, Z.; Wu, Y.-S.; Chen, Y. Exotic fractional topological states in a two-dimensional organometallic material. *Phys. Rev. B* **2014,** 89, (12), 125411-125411.
300. Regnault, N.; Bernevig, B. A. Fractional Chern Insulator. *Phys. Rev. X* **2011,** 1, (2), 21014-21014.
301. Wu, Y.-L.; Bernevig, B. A.; Regnault, N. Zoology of fractional Chern insulators. *Phys. Rev. B* **2012,** 85, (7), 75116-75116.
302. Wu, C.; Das Sarma, S. px,y-orbital counterpart of graphene: Cold atoms in the honeycomb optical lattice. *Phys. Rev. B* **2008,** 77, (23), 235107-235107.
303. Kobayashi, K.; Okumura, M.; Yamada, S.; Machida, M.; Aoki, H. Superconductivity in repulsively interacting fermions on a diamond chain: Flat-band-induced pairing. *Phys. Rev. B* **2016,** 94, (21), 214501-214501.
304. Mielke, A. Ferromagnetism in the Hubbard model on line graphs and further considerations. *J. Phys. A: Math. Gen.* **1991,** 24, (14), 3311-3321.

305. Mielke, A. Ferromagnetic ground states for the Hubbard model on line graphs. *J. Phys. A: Math. Gen.* **1991,** 24, (2), L73-L77.
306. Mielke, A. Exact ground states for the Hubbard model on the Kagome lattice. *J. Phys. A: Math. Gen.* **1992,** 25, (16), 4335-4345.
307. Tasaki, H. Ferromagnetism in the Hubbard models with degenerate single-electron ground states. *Phys. Rev. Lett.* **1992,** 69, (10), 1608-1611.
308. Zhang, S.; Hung, H.-h.; Wu, C. Proposed realization of itinerant ferromagnetism in optical lattices. *Phys. Rev. A* **2010,** 82, (5), 53618-53618.
309. Arita, R.; Shimoi, Y.; Kuroki, K.; Aoki, H. Flat-band ferromagnetism induced by off-site repulsions. *Phys. Rev. B* **1998,** 57, (17), 10609-10612.
310. Tang, E.; Mei, J.-W.; Wen, X.-G. High-Temperature Fractional Quantum Hall States. *Phys. Rev. Lett.* **2011,** 106, (23), 236802-236802.
311. Sethi, G.; Liu, F. Anomalous Quantum Hall Bilayer Effect. *arXiv:2211.04613* **2022**.
312. Liu, H.; Sethi, G.; Sheng, D. N.; Zhou, Y.; Sun, J.-T.; Meng, S.; Liu, F. High-temperature fractional quantum Hall state in the Floquet kagome flat band. *Phys. Rev. B* **2022,** 105, (16), L161108.
313. Liu, G.; Zhang, P.; Wang, Z.; Li, S.-S. Spin Hall effect on the kagome lattice with Rashba spin-orbit interaction. *Phys. Rev. B* **2009,** 79, (3), 35323-35323.
314. Guo, H. M.; Franz, M. Three-Dimensional Topological Insulators on the Pyrochlore Lattice. *Phys. Rev. Lett.* **2009,** 103, (20), 206805-206805.
315. Guo, H. M.; Franz, M. Topological insulator on the kagome lattice. *Phys. Rev. B* **2009,** 80, (11), 113102-113102.
316. Wang, Z.; Zhang, P. Quantum spin Hall effect and spin-charge separation in a kagomé lattice. *New J. Phys.* **2010,** 12, (4), 43055-43055.
317. Kurita, M.; Yamaji, Y.; Imada, M. Topological Insulators from Spontaneous Symmetry Breaking Induced by Electron Correlation on Pyrochlore Lattices. *J. Phys. Soc. Jpn.* **2011,** 80, (4), 44708-44708.
318. Hatsugai, Y.; Maruyama, I. ZQ topological invariants for Polyacetylene, Kagome and Pyrochlore lattices. *EPL (Europhysics Letters)* **2011,** 95, (2), 20003-20003.
319. Sun, K.; Gu, Z.; Katsura, H.; Das Sarma, S. Nearly Flatbands with Nontrivial Topology. *Phys. Rev. Lett.* **2011,** 106, (23), 236803-236803.
320. Wang, Z. F.; Su, N.; Liu, F. Prediction of a Two-Dimensional Organic Topological Insulator. *Nano Lett.* **2013,** 13, (6), 2842-2845.
321. Parameswaran, S. A.; Kimchi, I.; Turner, A. M.; Stamper-Kurn, D. M.; Vishwanath, A. Wannier Permanent Wave Functions for Featureless Bosonic Mott Insulators on the 1/3-Filled Kagome Lattice. *Phys. Rev. Lett.* **2013,** 110, (12), 125301-125301.
322. Zong, Y.; Xia, S.; Tang, L.; Song, D.; Hu, Y.; Pei, Y.; Su, J.; Li, Y.; Chen, Z. Observation of localized flat-band states in Kagome photonic lattices. *Opt. Express* **2016,** 24, (8), 8877-8877.
323. Ohgushi, K.; Murakami, S.; Nagaosa, N. Spin anisotropy and quantum Hall effect in the kagomé lattice: Chiral spin state based on a ferromagnet. *Phys. Rev. B* **2000,** 62, (10), R6065-R6068.
324. Gao, L.; Sun, J.-T.; Sethi, G.; Zhang, Y.-Y.; Du, S.; Liu, F. Orbital design of topological insulators from two-dimensional semiconductors. *Nanoscale* **2019,** 11, (47), 22743-22747.
325. Ni, X.; Zhou, Y.; Sethi, G.; Liu, F. π-Orbital Yin–Yang Kagome bands in anilato-based metal–organic frameworks. *Phys. Chem. Chem. Phys.* **2020,** 22, (44), 25827-25832.

326. Zhou, Y.; Sethi, G.; Zhang, C.; Ni, X.; Liu, F. Giant intrinsic circular dichroism of enantiomorphic flat Chern bands and flatband devices. *Phys. Rev. B* **2020,** 102, (12), 125115-125115.
327. Zhou, Y.; Sethi, G.; Liu, H.; Wang, Z.; Liu, F. Excited quantum anomalous and spin Hall effect: dissociation of flat-bands-enabled excitonic insulator state. *Nanotechnology* **2022,** 33, (41), 415001.
328. Cao, Y.; Fatemi, V.; Fang, S.; Watanabe, K.; Taniguchi, T.; Kaxiras, E.; Jarillo-Herrero, P. Unconventional superconductivity in magic-angle graphene superlattices. *Nature* **2018,** 556, (7699), 43-50.